Chemical Engineering Journal 524 (2025) 168929

Contents lists available at ScienceDirect

Chemical Engineering Journal

journal homepage: www.elsevier.com/locate/cej

Potential of high-temperature steam reforming for enabling DME as a hydrogen carrier

Timm Ruther [a,*], Hannes Stadler [a], Andreas Peschel [a,b,*]

[a] Forschungszentrum Jülich GmbH, Institute for a Sustainable Hydrogen Economy (INW), Jülich, Germany
[b] RWTH Aachen University, Aachener Verfahrenstechnik, Process and Plant Engineering for Chemical Hydrogen Storage, Aachen, Germany

ARTICLE INFO

Keywords:
Steam reforming
Renewable dimethyl ether
Carbon capture
DME/CO_2-cycle
Green hydrogen
Hydrogen carrier

ABSTRACT

In order to facilitate the importation of renewable hydrogen to Europe via dimethyl ether (DME), it is imperative to develop a robust steam reforming technology that is currently not available. This study explores the potential of state-of-the-art steam reforming technology of natural gas processing to address this technology gap, thereby facilitating accelerated commercialization. A process simulation was conducted in which a steam methane reformer (SMR) and a steam DME reformer with an integrated carbon capture unit (capture rate: 90 %) were modeled and compared in terms of efficiency, CO_2 emissions, feedstock consumption, hydrogen yield and energy demand. The steam DME reformer demonstrated a cold gas efficiency (CGE) of 70.9 %, accompanied by uncaptured carbon emissions (UCE) of 1.12 kg CO_2 per kg H_2, as compared to 73.0 % efficiency and 1.03 kg CO_2 per kg H_2 observed for the SMR. The performance of the amine scrubber had the most significant impact on both the CGE and the UCE. Although DME reforming exhibited slightly lower efficiency and higher feedstock and energy requirements, it consistently achieved higher hydrogen yields, underscoring its potential as a renewable hydrogen carrier. This work should therefore be regarded as a foundational baseline study, providing the first detailed reference point for renewable DME reforming and a basis for future research into optimized reforming conditions, advanced concepts, and alternative CO_2 capture strategies.

1. Introduction

Europe's high energy demand and its future reliance on renewable energy imports from regions such as Australia, Chile, and Africa necessitate efficient, high-density energy transport systems, like renewable hydrogen (H_2) [1,2]. However, the economic viability of compressed H_2 for long-range ship transport is questionable and pipeline transport not always feasible or economic for very long ranges [3,4]. Furthermore, liquid H_2 necessitates substantial energy consumption (10 to 13 kWh per kg of H_2 for liquefaction) and the development of new infrastructure [3,5,6]. Consequently, alternative hydrogen carriers such as renewable ammonia, methanol (MeOH), and dimethyl ether (DME) are being explored as more practical solutions for transportation and storage [7].

Renewable DME (rDME) has been discussed as an efficient H_2 carrier, with a high technical H_2 storage capacity of 26.1 wt%, which surpasses the capacities of MeOH (18.8 wt%) and ammonia (17.8 wt%) [8]. This attribute renders DME a significantly more energy-dense option for H_2 transport. Moreover, due to its analogous physical properties, DME is utilized as a blend-in or substitute for liquefied petroleum gas (LPG) [9,10] and diesel [11,12], and it can substitute for MeOH as a feedstock for hydrocarbon production [13].

Due to the disadvantage of DME containing carbon, Schühle et al. proposed a closed carbon cycle for green H_2 imports, in which CO_2 from the steam reforming of DME is captured, transported, and reused for DME synthesis in combination with green H_2 from electrolysis [8]. In their study, Schühle et al. demonstrated that the energy efficiency of the DME/CO_2 system is more energy efficient to that of the carbon-free hydrogen carrier ammonia (54.52 % DME; 49.75 % ammonia) system [8]. The synthesis of DME is a state-of-the-art process that necessitates adaptation to renewable feedstocks [14]. A hybrid tank concept is currently under developed by Mitsubishi Heavy Industries for the purpose of facilitating the transportation of carbon dioxide (CO_2) and LPG-like substances [15,16], such as DME.

The steam reforming of DME is a well-established concept that requires further development for large-scale hydrogen production to enable the DME/CO_2-cycle. Historically, this process has been predominantly explored at a modest scale within the context of fuel cells, operating at temperatures in the range of 300 °C [17,18]. A substantial

* Corresponding authors at: Forschungszentrum Jülich GmbH, Institute for a Sustainable Hydrogen Economy (INW), Jülich, Germany.
E-mail addresses: t.ruther@fz-juelich.de (T. Ruther), a.peschel@fz-juelich.de (A. Peschel).

https://doi.org/10.1016/j.cej.2025.168929
Received 6 June 2025; Received in revised form 4 September 2025; Accepted 24 September 2025
Available online 25 September 2025

Nomenclature

AS	Amine scrubber
ATR	Autothermal reformer
CGE	Cold gas efficiency
DAC	Direct air capture
DME	Dimethyl ether
E_{H_2}	Specific energy demand of hydrogen
e-SMR	Electrically heated steam methane reformer
FG	Flue gas
HL	Thermal loss
HP	High-pressure
HX	Heat exchanger
HX02	Feed preheater
HX03	Superheater
HX08	Hotbox
HX09	Steam superheater
HX10	Air preheater
HX11	Low-pressure steam generator
LHV	Lower heating value
LHV_{CH_4}	Lower heating value of methane
LHV_{DME}	Lower heating value of dimethyl ether
LHV_{feed}	Lower heating value of the feedstock
LHV_{H_2}	Lower heating value of hydrogen
LNG	Liquefied natural gas
LP	Low-pressure
LPG	Liquefied petroleum gas
LSNG	Liquefied synthetic natural gas
$\dot{m}_{CO_2,flue\ gas}$	Mass flow of carbon dioxide at the reformer outlet (plant) in the flue gas(es)
$\dot{m}_{feed}$	Mass flow of methane or dimethyl ether fed to the reformer (reactor)
$\dot{m}_{fuel}$	Mass flow of methane or dimethyl ether used as fuel for the burner(s)
$\dot{m}_{H_2,product}$	Mass flow of the hydrogen product stream at the reformer (plant) outlet
$m_{spec,feedstock}$	Specific feedstock demand
MeOH	Methanol
MT	Medium temperature
$\dot{n}_{CH_4,out}$	Methane molar flow rate at the reformer (reactor) outlet
$\dot{n}_{C_xH_yO_z,in}$	Methane or dimethyl ether molar flow rate at the reformer (reactor) inlet
$\dot{n}_{feed}$	Mole flow of methane or dimethyl ether fed to the reformer (reactor)
$\dot{n}_{feed}$	Mole flow of methane or dimethyl ether used as fuel for the burner(s)
$N_{H_2,max}$	Stoichiometric coefficient of hydrogen in the reforming reaction
$\dot{n}_{H_2,product}$	Mole flow of the hydrogen product stream at the reformer (plant) outlet
$\dot{n}_{H_2O,out}$	Water molar flow rate at the reformer (reactor) outlet
$\dot{n}_{overall,out}$	Overall molar flow rate at the reformer (reactor) outlet
NG	Natural gas
P	Power (electrical)
$P_{el,i}$	Electrical power demand of unit i
PSA	Pressure swing adsorption
Q	Thermal energy
rDME	Renewable dimethyl ether
RG	Regasifier
S1	First process gas separator
S2	Second process gas separator
S3	Flue gas separator
S/C	Steam-to-carbon ratio
S/C_{norm}	Normalized steam-to-carbon ratio
S/C_{stoi}	Stochiometric steam-to-carbon ratio
$S/C_{stoi,CH_4}$	Stoichiometric steam-to-carbon ratio for methane steam reforming
$S/C_{stoi,DME}$	Stoichiometric steam-to-carbon ratio for dimethyl ether steam reforming
SDR	Steam dimethyl ether reformer
SNG	Synthetic natural gas
SMR	Steam methane reformer
T_{MTWGS}	Medium temperature water-gas shift reactor outlet temperature
T_{outlet}	Reformer (reactor) outlet temperature
TRL	Technology readiness level
UCE	Uncaptured carbon dioxide emissions
WGS	Water-gas shift
WHB	Waste heat boiler
x	Number of carbon atoms per molecule
y	Number of hydrogen atoms per molecule
Y_{H_2}	Hydrogen yield
z	Number of oxygen atoms per molecule
η_{adia}	Adiabatic efficiency

amount of thermodynamic studies has been conducted over the past 25 years, demonstrating the thermodynamic feasibility of achieving a hydrogen yield approaching 100 % [19–21]. Consequently, there has been an increase in the interest surrounding the DME steam reforming process at larger-scale plants [8,22].

In summary, the low-temperature steam reforming of DME (R01) occurs in two reaction steps (R02, R03) via the intermediate MeOH [19,23,24]. The enthalpies of formation from literature (Table S1) were used to calculate the reaction enthalpies for all reactions in this article [25–31].

DME steam reforming $\left(\Delta H_r^0 = 122.6\ \frac{kJ}{mol}\right)$:

$$CH_3OCH_3 + 3H_2O \rightleftharpoons 2CO_2 + 6H_2 \quad (R01)$$

DME hydrolysis: $\left(\Delta H_r^0 = 24.1\ \frac{kJ}{mol}\right)$:

$$CH_3OCH_3 + H_2O \rightleftharpoons 2CH_3OH \quad (R02)$$

MeOH steam reforming $\left(\Delta H_r^0 = 49.3\ \frac{kJ}{mol}\right)$:

$$CH_3OH + H_2O \rightleftharpoons CO_2 + 3H_2 \quad (R03)$$

In the context of the DME steam reforming reaction (R01), a bifunctional catalyst system is employed. The DME hydrolysis (R02) is catalyzed by an acidic catalyst, mostly γ-Al_2O_3 or zeolites [32–35], while the MeOH steam reforming (R03) is predominantly catalyzed by a copper-based catalyst [32–37]. A range of other metals, including palladium, platinum, nickel, molybdenum, and zinc, are also being investigated [32,37–41]. Nonetheless, the catalysts employed in these studies have not been subjected to evaluation regarding their long-term stability [23,42–44]. In contrast, the catalysts that were subjected to testing for a duration exceeding 1000 h demonstrated a substantial degree of deactivation [45–47]. This outcome is a matter of significant concern for industrial processes.

The low technology readiness level (TRL) of the low-temperature steam reforming of DME (approx. 4 or 5) is primarily attributable to challenges in scaling up the process, mainly in optimizing the catalyst

performance, with particular emphasis on the long-term stability, and missing protypes for reactor and process evaluation.

A review of the pertinent literature reveals the existence of several concepts for DME steam reforming reactors, including gas-heated [22,48,49], steam-heated [22,50], electrical-heated [22], oil-heated [51,52], and burner-heated fixed-bed reactors [22], as well as fluidized-bed [22,53,54], microchannel [55,56], and membrane reactor concepts [57]. The primary design concept is analogous to the conventional MeOH steam reforming process [58,59], which has normally a hydrogen production capacity of around 1000 $Nm^3_{H_2}/h$ [51,52,60]. Among the proposed concepts only the "burner-heated fixed bed reactor" is a state-of-the-art process for large-scale steam reforming ($>100\ kNm^3_{H_2}/h$), the steam methane reformer (SMR) [61–63].

The history of SMR technology spans nearly 90 years, with its initial application in the processing of natural gas and subsequent adaptation to other feedstocks, including LPG [64]. In an SMR, methane undergoes a process of thermochemical reactions (R04, R06) within multiple tubes at temperatures ranging from 850 to 900 °C and pressures of 20 to 30 bar; the required heat is provided by burners [61,62]. Due to the high carbon monoxide (CO) content in the product, it is subsequently shifted with steam (R05) to H_2 and CO_2 in the water-gas shift (WGS) reactor, with the objective of increasing H_2 production [62]. Hydrogen separation is achieved through pressure swing adsorption (PSA) [61,62]. The three primary reactions (R04 to R06) involved in steam methane reforming are as follows [63]:

CH_4 steam reforming to CO ($\Delta H^0_r = 205.9\ \frac{kJ}{mol}$):

$$CH_4 + H_2O \rightleftharpoons CO + 3H_2 \quad \text{(R04)}$$

WGS reaction ($\Delta H^0_r = -41.2\ \frac{kJ}{mol}$):

$$CO + H_2O \rightleftharpoons CO_2 + H_2 \quad \text{(R05)}$$

CH_4 steam reforming to CO_2 ($\Delta H^0_r = 164.7\ \frac{kJ}{mol}$):

$$CH_4 + 2H_2O \rightleftharpoons CO_2 + 4H_2 \quad \text{(R06)}$$

To date, the application of an SMR for high-temperature DME steam reforming has not been subject of detailed investigations. Given the pivotal role of renewable hydrogen imports to Europe via the renewable DME, this study aims to address the knowledge gap by evaluating the high-temperature DME steam reforming concept as an alternative to the conventionally studied low-temperature steam reforming of DME in the context of the DME/CO_2-cycle for renewable hydrogen imports into Europe. This approach would enable expedited upscaling, attributable to a higher TRL of 9 for steam methane reformer technology.

The objective of this study is to conceptualize an SMR-based steam DME reformer (SDR) using liquefied rDME as feedstock and compare it with an SMR using liquefied synthetic natural gas (LSNG) as feedstock (Fig. 1). The purpose of this comparison is to assess the feasibility of adapting the steam reforming process to DME (Fig. 1). To enable the back-shipping of CO_2, the integration of a carbon capture unit is essential. Here, an amine scrubber (AS) for flue gas carbon capture, recognized as the state-of-the-art technology for achieving an overall CO_2 capture rate of 90 %, was incorporated into the process (Fig. 1) [65,66]. This work should therefore be regarded as a systematic baseline for high-temperature SDR, providing the necessary reference point for future investigations into autothermal reforming, electrically heated reforming, and low-temperature pathways.

2. Simulation approach

This work investigates two process configurations for H_2 production, an SMR and an SDR. All simulations in this study were conducted using AVEVA™ Process Simulation 2024.2 software.

In the context of steam reforming, the steam-to-carbon ratio (S/C) has been shown to be a pivotal parameter, along with pressure and temperature [63]. S/C is defined as the ratio of water molecules to carbon atoms in the reactor feed. This concept is applicable to hydrocarbons, including methane, and their oxygen-containing derivatives, such as DME. With x, y, z representing the number of carbon, hydrogen, and oxygen atoms per molecule, respectively, the steam-to-carbon ratio can be expressed as follows (see also SE1 and SE2):

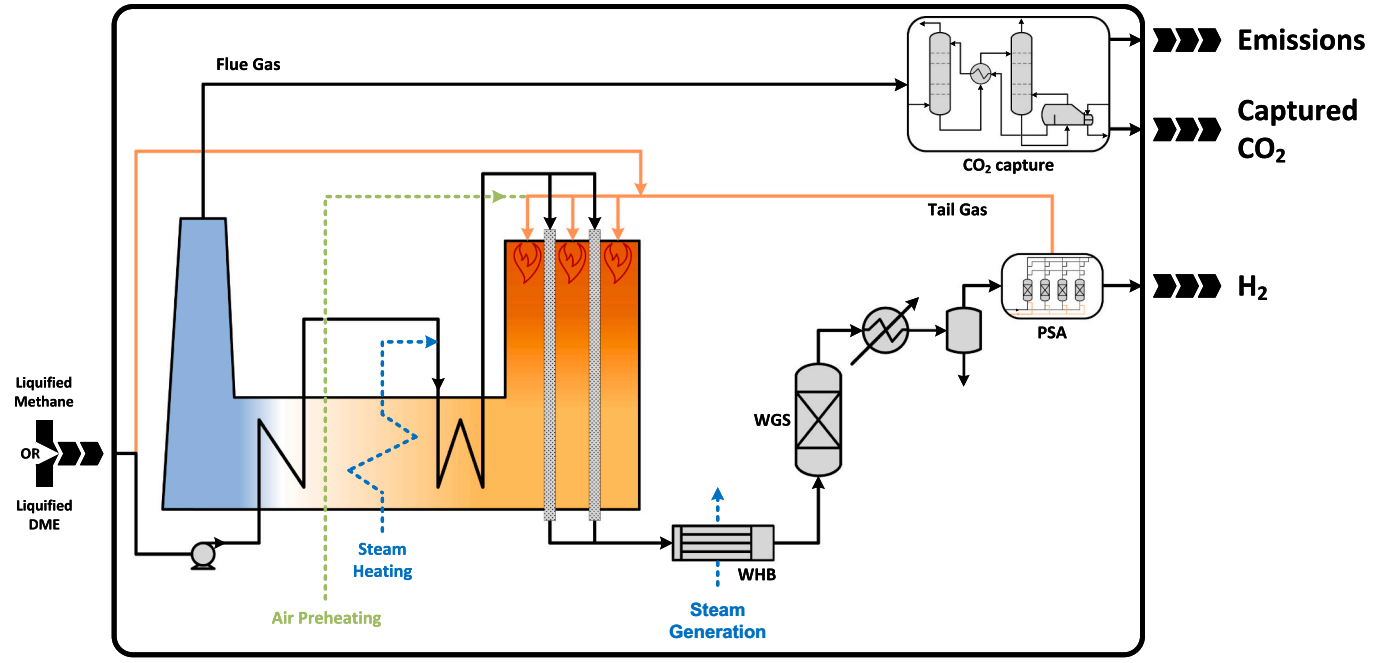

Fig. 1. Abridged scheme of the steam reforming process with carbon capture using liquefied DME or LNG as feedstock for the production of hydrogen.

$$S/C = \frac{\dot{n}_{H_2O,in}}{\dot{n}_{C_xH_yO_z,in} * x} \quad \text{(E1)}$$

The stoichiometrically required S/C for complete conversion to H_2 and CO_2 (S/C_{stoi}) differs between the steam reforming of DME and CH_4: $S/C_{stoi,DME} = 1.5\ \frac{mol_{H_2O}}{mol_{DME}}$ (SE3); $S/C_{stoi,CH_4} = 2\ \frac{mol_{H_2O}}{mol_{CH_4}}$ (SE4). For better comparison of both reactions, a normalized steam to carbon ratio is introduced in this study:

$$S/C_{norm} = \frac{S/C}{S/C_{stoi}} \quad \text{(E2)}$$

While thermodynamic data for the steam reforming of CH_4 is available within the commercially operated pressure range of 10 to 30 bar [61–63], the published thermodynamic data for steam reforming of DME is only available for lower pressures (1 to 5 bar) [19,21]. However, given the expense associated with hydrogen compression [67], it is advantageous to consider reforming under pressures of 20 to 30 bar for DME as well. Consequently, a preliminary thermodynamic evaluation of the DME steam reforming shows the feasibility.

2.1. Thermodynamic evaluation

Thermodynamic equilibrium calculations for the steam reforming of DME are performed using a Gibbs Minimization Reactor and the Peng-Robinson equation-of-state [68]. Molar compositions are analyzed at varying temperatures (300 to 1000 °C) at 20 bar with an S/C_{norm} of 1. The system included CO_2, CO, H_2, DME, MeOH, and H_2O (Fig. 2A), with a separate simulation incorporating also CH_4 (Fig. 2B), which can be formed via CO and CO_2 methanation (reverse of R04 and R06) [69] or DME decomposition (R07) [70,71].

DME decomposition to CH_4, CO, and H_2 ($\Delta H_r^0 = -1.0\ \frac{kJ}{mol}$):

$$CH_3OCH_3 \rightleftharpoons CH_4 + CO + H_2 \quad \text{(R07)}$$

Classical nickel-based SMR catalysts have been shown to promote methanation [72]. However, the steam reforming of CH_4 requires higher reaction temperatures than the low-temperature steam reforming of DME is normally operated. Therefore, it is of interest to suppress methane formation in low-temperature steam reforming, with the objective of achieving a high hydrogen yield [40,73].

As demonstrated in Fig. 2, both graphs illustrate that across the temperature range of 400 to 1000 °C the DME and MeOH mole fractions are minimal, with values less than 0.05 mol% in the dry gas. The primary distinction between scenarios A and B is that, in scenario B, where methane is in equilibrium, temperatures exceeding 800 °C are necessary to achieve substantial conversions to H_2. In scenario A, the hydrogen mole fraction exceeds 65 mol% in the dry gas throughout the entire temperature range. Of particular interest are the temperatures below 500 °C. This is attributable to the fact that the process of heat recovery is less complicated due to the reduced energy requirements, which are a consequence of the diminished temperature level. However, at temperatures below 400 °C, the MeOH and DME mole fractions increase steeply, yet remain below 0.4 mol% at 300 °C. Additionally, kinetic hindrance is predicted at low temperatures, which may result in thermodynamically feasible conversion rates not being attained [74].

Conversely, classical steam reforming of CH_4 has been demonstrated to attain near thermodynamic equilibrium at elevated temperatures (>800 °C), with the equilibrium being predominantly influenced by the reformer's outlet temperature [61]. A similar outcome is anticipated for the steam reforming of DME at elevated temperatures. Similar as in classical SMR design, the overall reaction is not kinetically limited but by the heat transfer from the burner into the reaction zone, thereby enabling the highly endothermic reaction.

In consideration of the literature of CH_4 formation over nickel catalysts [72], the inclusion of CH_4 in the reaction scheme depicted in Fig. 2B is deemed essential for systems employing state-of-the-art nickel-based SMR catalysts, which compared to the developed low-temperature catalysts have a high long-time stability of several years [75,76]. The data suggest that the steam reforming of DME occurs via CH_4 as an intermediate. However, the precise reaction mechanism remains to be elucidated, and no experimental data is currently available for the steam reforming of DME over SMR catalysts.

Consequently, it is anticipated that the steam reforming of DME with a nickel-based catalyst will require elevated temperatures, similar to those necessary for the steam reforming of CH_4. Given the very low concentrations of DME and MeOH ($<10^{-6}$), it is anticipated that complete conversion of DME and MeOH will occur. However, a certain CH_4 slip can occur, similar to CH_4 steam reforming. Consequently, this key performance indicator of an SMR should be applied to the high-temperature DME reforming as well. The CH_4 slip is defined as the mole fraction of CH_4 in the dry gas at the reactor outlet.

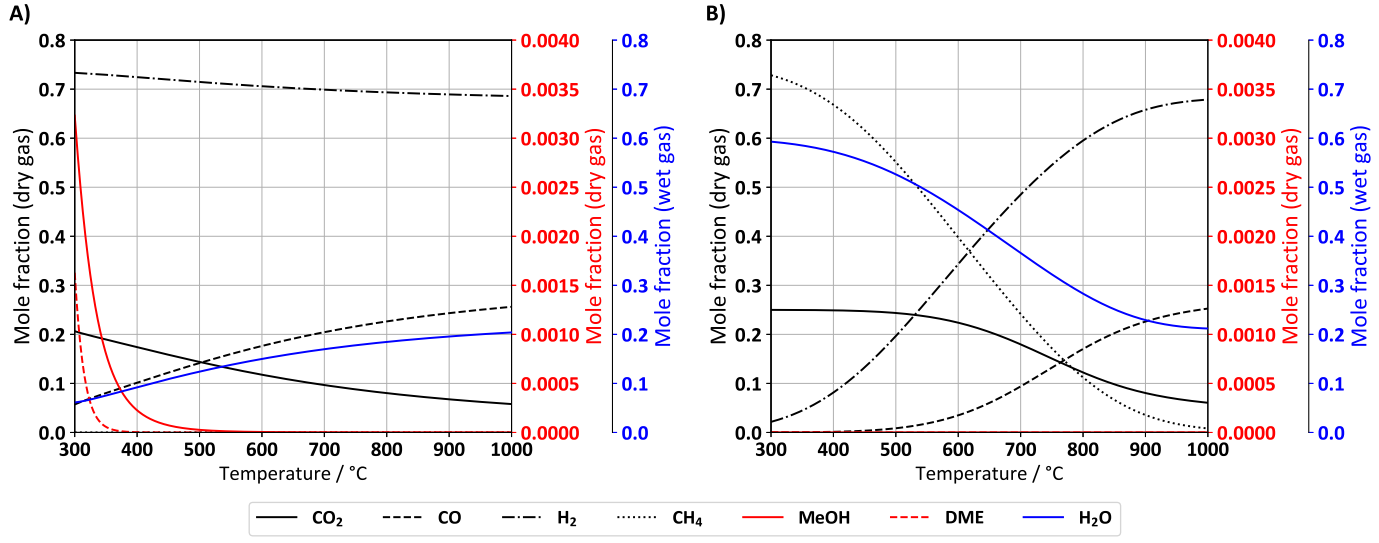

Fig. 2. DME steam reforming composition at thermodynamic equilibrium at 20 bar and $S/C_{norm} = 1$ from 300 to 1000 °C; A) excluding methane; B) including methane (the DME and MeOH mole fractions are always below 10^{-6}).

$$CH_4\ \text{slip} = \frac{\dot{n}_{CH_4,out}}{\dot{n}_{overall,out} - \dot{n}_{H_2O,out}} \quad \text{(E3)}$$

A comparison was made between CH_4 and DME steam reforming, with the CH_4 slip for both reactions being simulated at four distinct pressure-S/C_{norm}-combinations over the temperature range of 300 to 1000 °C. The results of these simulation are shown in Fig. 3.

The same trends for the CH_4 slip are observable for CH_4 and DME: lowering the pressure, increasing the temperature, and increasing S/C_{norm} leads to less CH_4 in the product stream. While the CH_4 slip reaches nearly 100 % for CH_4 at 300 °C, the maximum for DME is 75 %. This disparity can be attributed to the fact that the decomposition of DME to CH_4 and CO_2 results in the formation of one mole of CO_2 for every three moles of CH_4.

DME decomposition to CH_4 and CO_2 ($\Delta H_r^0 = -124.5\ \frac{kJ}{mol}$):

$$CH_3OCH_3 \rightleftharpoons 1.5CH_4 + 0.5CO_2 \quad \text{(R08)}$$

A typical methane slip of an SMR ranges from 3 to 8 % [61], corresponding to a temperature of approximately 750 to 1000 °C at 30 bar. As illustrated in Fig. 3, the CH_4 slip in DME steam reforming is comparable for the high temperature region to CH_4. The data presented in Fig. 3 supports the hypothesis that the high-temperature steam reforming of DME differs from the steam reforming of CH_4, primarily due to the process of DME decomposition to CH_4, which occurs at temperatures above 500 °C without catalyst [70,71], while the latter steam reforming of CH_4 remains constant. Consequently, the adaptation of SMR technology to DME appears to be a promising approach.

2.2. Process simulation methodology

In order to facilitate an optimal comparison of an SMR and an SDR simulation model, both were configured identical wherever possible. Both simulations are based on the top-fired reformer design by Linde [77] and both layouts use the PSA tail gas and part of the feedstock as fuel for the burners. The flow diagrams of the SMR and SDR are shown in Figs. 4 and 5, respectively. The corresponding stream information is displayed in Tables 1 and 2. The Steam Tables were used for the pure low-pressure (LP) steam system [78] and the Peng-Robinson equation-of-state for all other streams [68]. The H_2 production capacity for both systems is fixed at 200 $kNm^3_{H_2}/h$ with a purity of 99.999 % (10 ppm CO) and a pressure of 26.7 bar.

The LSNG feed is to be at bubble point at standard atmospheric pressure, which corresponds to a temperature of approximately −162 °C. The liquid DME is to be at bubble point at 20 °C, and the corresponding pressure is approximately 5.1 bar. Given the high purity specifications of fossil LNG (99.8 % CH_4) [79] and fossil DME (98.8 % DME) [80], and the absence of a defined composition for rDME and LSNG, the feedstocks were modeled as pure components (CH_4 and DME). This approach also facilitates a more effective comparison between the feedstocks CH_4 and DME. Given the low sulfur concentrations present in LSNG and rDME as compared to natural gas, desulfurization pretreatment of the feedstock is not incorporated in the models.

In the absence of an amine scrubber, an SMR typically generates export steam [61]. In this particular instance, however, no export steam is generated. Instead, the additional thermal energy is utilized to produce low-pressure steam (3 bar, approximately 134 °C), which is then used in the reboiler of the amine scrubber (HX13). This approach facilitates the comparison of the energy balance of both systems by eliminating the need to consider an additional product stream. In the context of a real-world plant, the option for steam export is likely to be incorporated with the objective of enhancing flexibility in addressing scenarios involving catalyst deactivation and plant maloperation.

It is noteworthy that both systems utilize an isothermal medium-temperature (MT) WGS reactor, a choice that is based on the reactor's enhanced operational flexibility, particularly for subsequent parameter

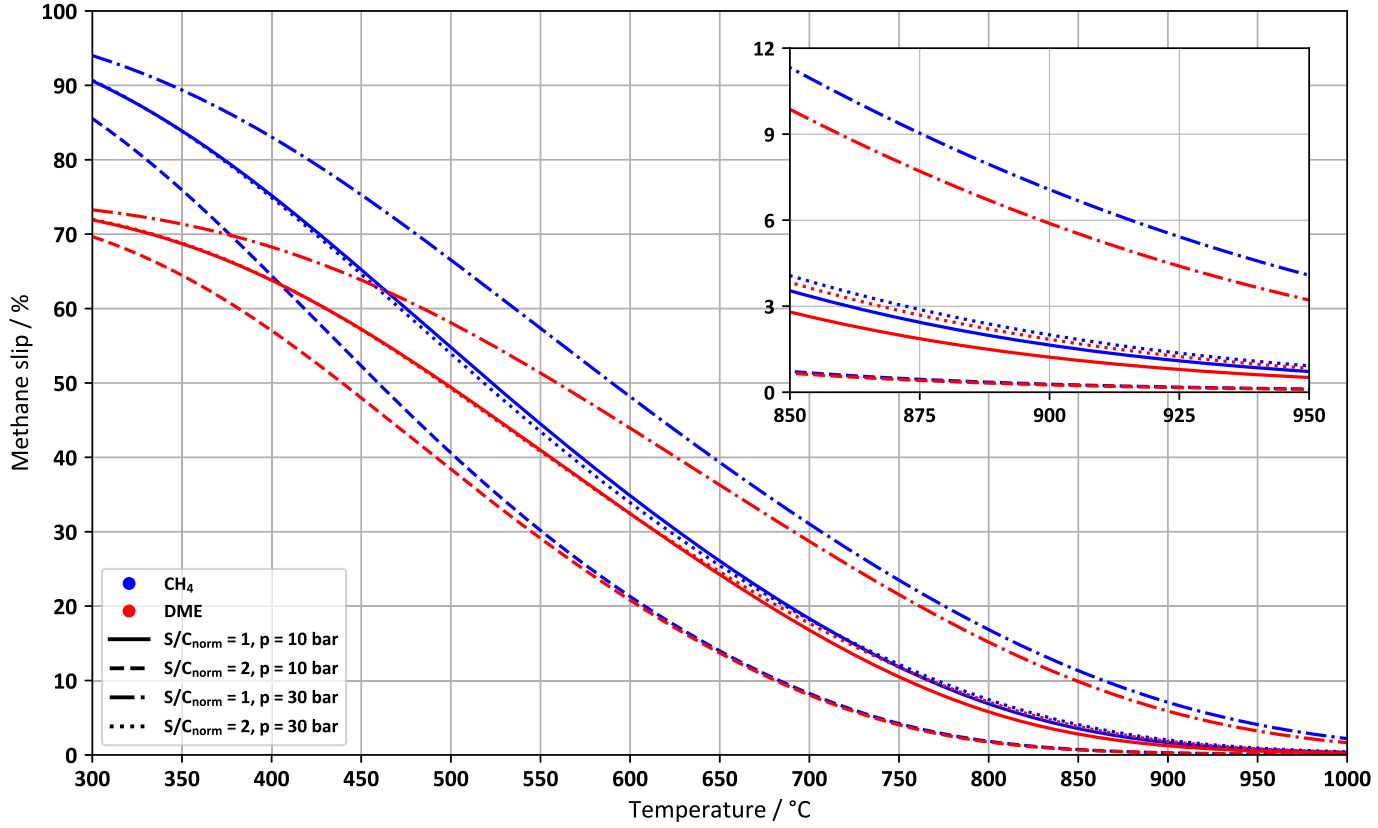

Fig. 3. Methane slips for CH_4 and DME steam reforming at different pressures, normalized S/Cs, and temperatures.

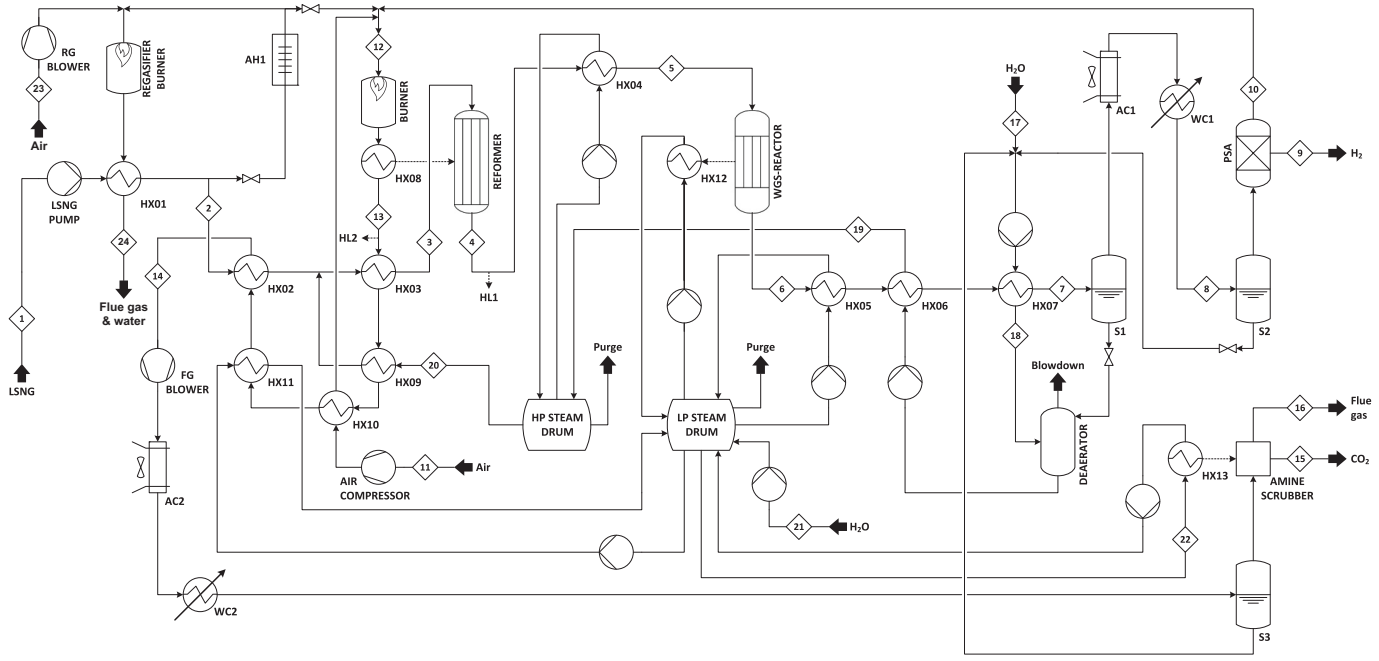

Fig. 4. Process flow diagram of the SMR simulation.

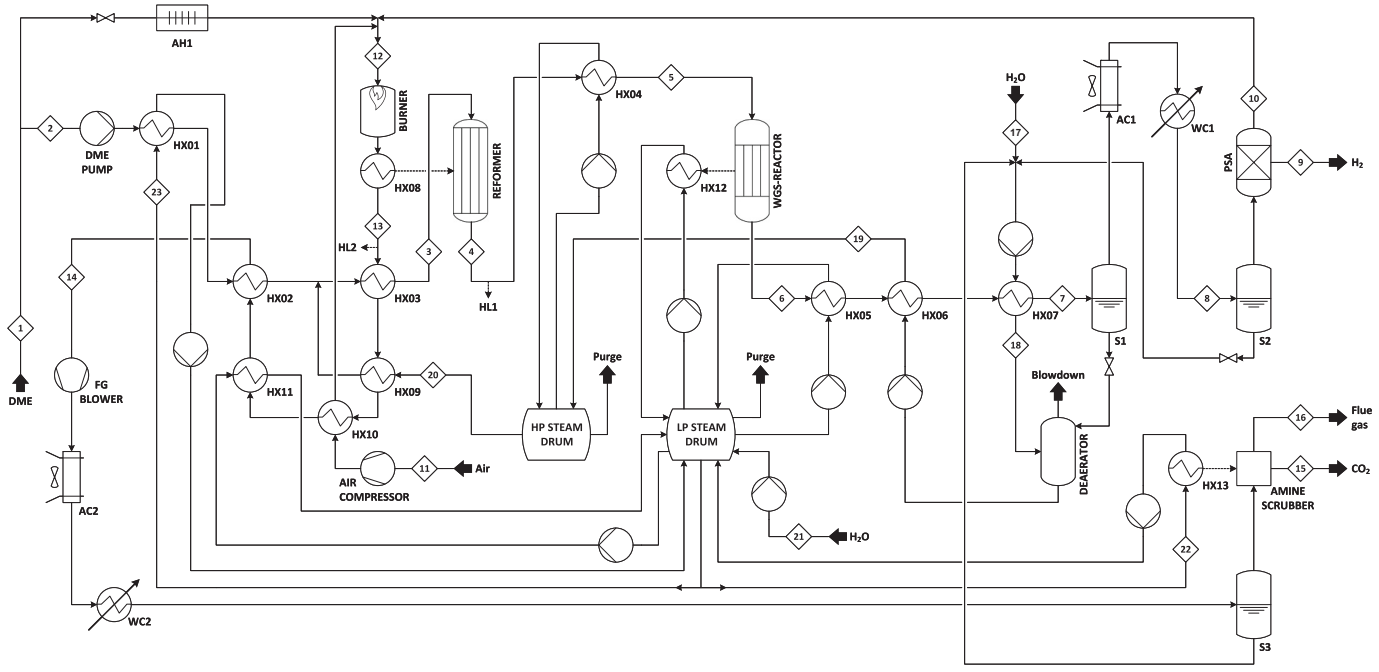

Fig. 5. Process flow diagram of the SDR simulation.

studies. This enhanced flexibility can be attributed to the fact that the allowable S/Cs for MT-WGS reactors are lower in comparison to the high-temperature WGS [81].

The reformer and MT-WGS reactor are modeled as Gibbs Minimization Reactors, while the burners are Conversion Reactors. The reformers are modeled with CH_4, MeOH, DME, H_2O, H_2, CO, and CO_2 as active components, while in the MT-WGS reactors MeOH, H_2O, H_2, CO, and CO_2 are considered. The burner converts 100 % of CH_4, MeOH, DME, H_2, and CO through the following combustion reactions (R09–R13).

$$CH_4 + 2O_2 \rightarrow CO_2 + 2H_2O \quad \text{(R09)}$$

$$CH_3OH + 1.5O_2 \rightarrow CO_2 + 2H_2O \quad \text{(R10)}$$

$$CH_3OCH_3 + 3O_2 \rightarrow 2CO_2 + 3H_2O \quad \text{(R11)}$$

$$H_2 + 0.5O_2 \rightarrow H_2O \quad \text{(R12)}$$

$$CO + 0.5O_2 \rightarrow CO_2 \quad \text{(R13)}$$

In order to ensure complete combustion, it is imperative to supply 8 to 10 % excess air for an SMR [82]. In this instance, 8 % excess air is assumed, as a result of the absence of higher hydrocarbons in the feed [61].

Table 1
Stream data from the SMR simulation (Fig. 4).

Stream number	1	2	3	4	5	6	7	8	9	10	11	12
T / °C	−162	15.0	650	900	310	270	124	40.0	44.1	23.9	20.0	387
p / bar	1.01	32.4	32.0	30.0	29.8	28.3	27.7	27.4	26.7	1.01	1.01	1.01
$\dot{n}$ / kmol/s	1.02	0.878	3.17	4.63	4.63	4.61	4.61	4.09	2.48	1.26	3.99	5.37
$\dot{m}$ / kg/s	16.4	14.1	55.4	55.4	55.4	55.4	55.4	46.0	4.99	34.6	116	152
Component mole fractions												
H_2O	0.000	0.000	0.720	0.289	0.289	0.190	0.190	0.087	0.000	0.009	0.000	0.002
Ar	0.000	0.000	0.000	0.000	0.000	0.000	0.000	0.000	0.000	0.000	0.009	0.007
DME	0.000	0.000	0.000	0.000	0.000	0.000	0.000	0.000	0.000	0.000	0.000	0.000
O_2	0.000	0.000	0.000	0.000	0.000	0.000	0.000	0.000	0.000	0.000	0.210	0.155
N_2	0.000	0.000	0.000	0.000	0.000	0.000	0.000	0.000	0.000	0.000	0.781	0.579
CO_2	0.000	0.000	0.000	0.048	0.048	0.149	0.149	0.167	0.000	0.544	0.000	0.128
CO	0.000	0.000	0.000	0.110	0.110	0.008	0.008	0.009	0.000	0.028	0.000	0.007
H_2	0.000	0.000	0.000	0.520	0.520	0.618	0.618	0.697	1.000	0.294	0.000	0.069
MeOH	0.000	0.000	0.002	0.000	0.000	0.002	0.002	0.002	0.000	0.002	0.000	0.001
CH_4	1.000	1.000	0.277	0.033	0.033	0.034	0.034	0.038	0.000	0.123	0.000	0.053
Stream number	13	14	15	16	17	18	19	20	21	22	23	24
T / °C	1050	150	43.6	43.6	20.0	94.8	134	239	20.0	134	20.0	45.0
p / bar	1.01	0.961	1.01	1.01	1.01	1.01	32.4	32.4	1.01	3.00	1.01	1.01
$\dot{n}$ / kmol/s	5.17	5.17	0.91	3.64	0.83	1.80	2.31	2.29	0.00234	2.34	0.17	0.19
$\dot{m}$ / kg/s	152	152	40.0	101	14.9	32.6	41.8	41.4	0.0422	42.2	4.89	5.15
Component mole fractions												
H_2O	0.184	0.184	0.000	0.091	1.000	0.996	0.997	0.997	1.000	1.000	0.000	0.177
Ar	0.007	0.007	0.000	0.010	0.000	0.000	0.000	0.000	0.000	0.000	0.009	0.008
DME	0.000	0.000	0.000	0.000	0.000	0.000	0.000	0.000	0.000	0.000	0.000	0.000
O_2	0.012	0.012	0.000	0.017	0.000	0.000	0.000	0.000	0.000	0.000	0.210	0.014
N_2	0.602	0.602	0.002	0.855	0.000	0.000	0.000	0.000	0.000	0.000	0.781	0.711
CO_2	0.195	0.195	0.998	0.028	0.000	0.000	0.000	0.000	0.000	0.000	0.000	0.089
CO	0.000	0.000	0.000	0.000	0.000	0.000	0.000	0.000	0.000	0.000	0.000	0.000
H_2	0.000	0.000	0.000	0.000	0.000	0.000	0.000	0.000	0.000	0.000	0.000	0.000
MeOH	0.000	0.000	0.000	0.000	0.000	0.004	0.003	0.003	0.000	0.000	0.000	0.000
CH_4	0.000	0.000	0.000	0.000	0.000	0.000	0.000	0.000	0.000	0.000	0.000	0.000

The reformers operate at an outlet temperature of 900 °C (with a 150 °C higher bridge wall temperature), an S/C_{norm} of 1.3, and an exit pressure of 30 bar with a 2 bar pressure drop [60–63]. The required heat is supplied by the hotbox (HX08). The model incorporates a temperature decline of 10 °C due to heat losses in the reformer pigtails (HL1). The MT-WGS reactors operate at an exit temperature of 270 °C, accompanied by a pressure drop of 1.5 bar [83,84]. The heat from the exothermic reaction is utilized by the heat exchanger HX12 for low-pressure steam generation.

The primary distinction between the SMR (Fig. 4) and SDR (Fig. 5) configuration is the feedstock supply; all other components of the setup are analogous. In the case of the SMR, the LSNG is pumped and regasified ($T = 15$ °C) in a submerged combustion vaporizer [85], the most flexible regasifier, with approximately 1.6 % of the LSNG being consumed as fuel. A portion of the gaseous CH_4 functions as a burner fuel for the SMR, while the remainder is introduced into the SMR and subsequently heated to approximately 148 °C within the flue gas channel. The fuel for both burners (the SMR and the regasifier) is subjected to pressure reduction and heated to 10 °C using a natural draft air heater. In the case of the SDR, the majority of the liquid DME is pumped above process pressure, evaporated with low-pressure steam, and further preheated by flue gas to approximately 133 °C. A smaller portion (approx. 9.1 %) is pressure-reduced, evaporated, and heated to 10 °C via a natural draft air heater. This smaller portion is then used as make-up fuel for the burner. The gaseous feedstock (CH_4 or DME) is subsequently mixed with superheated steam (500 °C) and is then further heated to 650 °C in the superheater HX03, after which it is fed to the reformer [63].

In the waste heat boiler (WHB) HX04, the product stream is cooled, generating high-pressure steam (32.4 bar, approx. 239 °C) for the reformer. Thereafter, the cooled product passes through the MT-WGS reactor and undergoes a three-step cooling process (HX05 to HX07). A two-stage separation (S1 and S2) with air (cooling to 70 °C) and water intercooling (cooling to 40 °C) isolates the liquid phase for the high-pressure steam system, while the gas phase enters the PSA unit, which is modeled as a split with 87 % hydrogen recovery [62] (99.999 % H_2, 10 ppm CO). The PSA tail gas is subsequently mixed with make-up fuel and air for combustion in the burner.

The flue gas (FG) heat is utilized in multiple units, including: the HX08 (hotbox), HX03 (superheater), HX09 (steam superheater), HX10 (air preheater), HX11 (LP steam generator), and HX02 (feed preheaters) down to 150 °C. At the end of the hotbox (bridge wall temperature), the transition to the convection zone is modeled as a thermal loss (HL2) of 10 °C.

The flue gas is pulled through the heat recovery by the flow gas blower and is subsequently cooled to 40 °C to be separated into its liquid and gas phase (S3). The liquid phase is subsequently introduced into the high-pressure steam system's make-up water, while the gas is directed into the amine scrubber, which is modeled as a split with 90 % CO_2 recovery (99.8 % CO_2, 0.2 % N_2) [86,87]. The CO_2-product pressure is set at 1 atm. The residual flue gas then exits the plant with the remaining CO_2 that has not been captured. The required amine scrubber reboiler duty for systems such as e.g. BASF's OASE® process and Shell's CANSOLV® process is reported in the literature to range from 2.0 to 2.6 GJ per tonne CO_2 [86–91]. In this study, a mean value of 2.3 is employed.

In the high-pressure steam system, make-up water is mixed with condensates from the secondary process gas separator (S2) and the flue gas separator (S3). The mixture is subsequently pumped and heated in the heat exchanger HX07 to approximately 95 °C before entering the deaerator alongside condensate from the primary process gas separator (S1). The deaerator is operated at 1 atm with a blowdown equal to 0.5 mol% of the water exiting. Subsequently, the water is pumped,

Table 2
Stream data from the SDR simulation (Fig. 5).

Stream number	1	2	3	4	5	6	7	8	9	10	11	12
T / °C	20.0	20.0	650	900	358	270	125	40.0	44.4	23.3	20.0	207
p / bar	5.10	5.10	32	30	29.8	28.3	27.7	27.4	26.7	1.01	1.01	1.01
ṅ / kmol/s	0.636	0.578	2.84	4.90	4.90	4.87	4.87	4.41	2.48	1.54	3.45	5.04
ṁ / kg/s	29.3	26.6	67.6	67.6	67.6	67.6	67.6	59.3	4.99	47.1	99.8	150
Component mole fractions												
H_2O	0.000	0.000	0.793	0.300	0.300	0.176	0.176	0.090	0.000	0.008	0.000	0.002
Ar	0.000	0.000	0.000	0.000	0.000	0.000	0.000	0.000	0.000	0.000	0.009	0.006
DME	1.000	1.000	0.203	0.000	0.000	0.000	0.000	0.000	0.000	0.000	0.000	0.011
O_2	0.000	0.000	0.000	0.000	0.000	0.000	0.000	0.000	0.000	0.000	0.210	0.143
N_2	0.000	0.000	0.000	0.000	0.000	0.000	0.000	0.000	0.000	0.000	0.781	0.534
CO_2	0.000	0.000	0.000	0.071	0.071	0.198	0.198	0.218	0.000	0.625	0.000	0.191
CO	0.000	0.000	0.000	0.139	0.139	0.010	0.010	0.012	0.000	0.033	0.000	0.010
H_2	0.000	0.000	0.000	0.462	0.462	0.585	0.585	0.646	1.000	0.241	0.000	0.073
MeOH	0.000	0.000	0.003	0.000	0.000	0.003	0.003	0.003	0.000	0.002	0.000	0.001
CH_4	0.000	0.000	0.000	0.029	0.029	0.029	0.029	0.032	0.000	0.091	0.000	0.028

Stream number	13	14	15	16	17	18	19	20	21	22	23
T / °C	1050	150	44.9	44.9	20.0	95.1	134	239	20.0	134	134
p / bar	1.01	0.961	1.01	1.01	1.01	1.01	32.4	32.4	1.01	3.00	3.00
ṅ / kmol/s	4.89	4.89	1.15	3.22	0.92	1.84	2.29	2.26	0.00327	2.96	0.313
ṁ / kg/s	150	150	50.5	89.6	16.6	33.3	41.3	40.9	0.0590	53.3	5.65
Component mole fractions											
H_2O	0.172	0.172	0.000	0.098	1.000	0.995	0.996	0.996	1.000	1.000	1.000
Ar	0.007	0.007	0.000	0.010	0.000	0.000	0.000	0.000	0.000	0.000	0.000
DME	0.000	0.000	0.000	0.000	0.000	0.000	0.000	0.000	0.000	0.000	0.000
O_2	0.011	0.011	0.000	0.017	0.000	0.000	0.000	0.000	0.000	0.000	0.000
N_2	0.550	0.550	0.002	0.836	0.000	0.000	0.000	0.000	0.000	0.000	0.000
CO_2	0.260	0.260	0.998	0.040	0.000	0.000	0.000	0.000	0.000	0.000	0.000
CO	0.000	0.000	0.000	0.000	0.000	0.000	0.000	0.000	0.000	0.000	0.000
H_2	0.000	0.000	0.000	0.000	0.000	0.000	0.000	0.000	0.000	0.000	0.000
MeOH	0.000	0.000	0.000	0.000	0.000	0.005	0.004	0.004	0.000	0.000	0.000
CH_4	0.000	0.000	0.000	0.000	0.000	0.000	0.000	0.000	0.000	0.000	0.000

preheated in heat exchanger HX06 to approximately 134 °C, and fed into the HP steam drum. The drum is operated at a circulation ratio of 12.5 and a purge equal to 1 mol% of the generated steam. The selected circulation ratio (SE6) is contingent upon the operational pressure of the steam drum [92,93]. In the low-pressure steam system, make-up water is directly pumped into the LP steam drum, which is operated at a circulation rate of 50 and a purge equal to 0.1 mol% of the generated steam. All utilities are modeled at ambient conditions of 1 atm and 20 °C. The molar composition used for air was: 78.08 % N_2, 20.95 % O_2, 0.93 % Ar, and 0.04 % CO_2.

3. Results and discussion

3.1. Process performance and validation

The most widely used parameter for evaluating the efficiency of an SMR is the cold gas efficiency (CGE), which is defined as follows based on the lower heating values (LHVs) and the mass flows of the H_2 product and the feed at the plant inlet (stream 1, Figs. 4 and 5):

$$CGE = \frac{\dot{m}_{H_2,product} * LHV_{H_2}}{\left(\dot{m}_{feed} + \dot{m}_{fuel}\right) * LHV_{feed}} \quad (E4)$$

The LHVs for H_2, CH_4, and DME are: $LHV_{H_2} = 119.96\ \frac{MJ}{kg}$ [94], $LHV_{CH_4} = 50.03\ \frac{MJ}{kg}$ [95], $LHV_{DME} = 28.84\ \frac{MJ}{kg}$ [95]. The latter two were derived from the standard net enthalpy of combustion values (SE7 and Table S2).

In the context of the closed DME/CO_2 cycle - particularly relevant for the transport of the hydrogen carrier - the required feedstock mass per unit mass of hydrogen, $m_{spec,feedstock}$, (E5) is a key metric.

$$m_{spec,feedstock} = \frac{\dot{m}_{feed} + \dot{m}_{fuel}}{\dot{m}_{H_2,product}} \quad (E5)$$

Beyond the feedstock requirement, the hydrogen yield, Y_{H_2}, (E6) is a key performance indicator, representing the fraction of the theoretically maximum producible hydrogen that is ultimately obtained as product. The feedstock specific factor $N_{H_2,max}$ being the stoichiometric coefficients in the reaction eqs. R06 and R01: $N_{H_2,max,CH_4} = 4$ and $N_{H_2,max,DME} = 6$.

$$Y_{H_2} = \frac{\dot{n}_{H_2,product}}{N_{H_2,max} * \left(\dot{n}_{feed} + \dot{n}_{fuel}\right)} \quad (E6)$$

The required energy demand per unit mass of hydrogen, E_{H_2}, (E7) is also a commonly used metric in the context of reforming:

$$E_{H_2} = \frac{\left(\dot{m}_{feed} + \dot{m}_{fuel}\right) * LHV_{feed} + \sum_i P_{el,i}}{\dot{m}_{H_2,product}} \quad (E7)$$

Another important parameter is the amount of uncaptured CO_2 per H_2. The uncaptured CO_2 emissions (UCE) are defined as follows:

$$UCE = \frac{\dot{m}_{CO_2,flue\ gas}}{\dot{m}_{H_2,product}} \quad (E8)$$

The process remains effectively carbon-neutral even without CO_2 capture, as the CO_2 released during reforming originates from renewable feedstocks such as rDME or SNG rather than fossil sources. Nevertheless, assessing carbon capture at this stage remains important, since the energy demand for reformer-integrated CO_2 capture is significantly lower than for the most widely studied alternative, direct air capture (DAC).

Schühle et al. reported energy requirements of 1.8 GJ (electrical) and 5.4 GJ (thermal) per tonne CO_2 for DAC [96], far exceeding those of conventional amine scrubbing - approximately 0.1 GJ (electrical) [94] and 2.3 GJ (thermal) per tonne CO_2. Accordingly, while emissions from renewable feedstocks do not represent a net fossil emission, their capture remains beneficial from an efficiency standpoint within the closed DME/CO_2-cycle. In this context, UCE should therefore be interpreted not as a climate burden but as a capture burden.

Table 3 presents the results from both simulations and literature data for an SMR with a carbon capture rate of 90 % (case 3 of the 2017 IEAGHG report [94]). The percentage of UCE from the regasification unit (RG) of the SMR is also included.

The SMR examined in this study exhibited an approximate 5.6 % higher CGE and a roughly 4.0 % higher UCE in comparison to the SMR documented by the IEAGHG [94]. Additionally, the results for $m_{spec,feedstock}$ and E_{H_2} of the SMR are in close agreement with literature values, with the specific feedstock demand approximately 12.1 % lower and the specific energy demand 4.9 % lower. The observed discrepancy in performance can be attributed to the methodology employed in the IEAGHG report, wherein electricity was produced using surplus steam [94]. Additionally, fossil natural gas (NG) was used as the feedstock in lieu of LSNG, thereby eliminating the requirement for a regasification process [94]. While the utilization of NG as opposed to LSNG results in an augmentation of the CGE, the generation of electricity from steam exerts a more substantial downward influence on the CGE compared to this study. The SMR results in this study are therefore consistent with the literature data, thereby validating the SMR methodology.

In comparison, the SDR is 2.6 % less efficient and generates 6.7 % more UCE than the SMR. This phenomenon can be attributed to the elevated levels of CO_2 generation resulting from the DME reactions in comparison to the CH_4 reactions. Specifically, the DME steam reforming reaction (R01) yields 0.33 mol of CO_2 per mole of H_2, while the steam reforming of CH_4 (R06) generates only 0.25 mol of CO_2 per mole of H_2. Furthermore, the combustion of DME (R11) yields a lower energy output compared to the combustion of CH_4 (R09), with 664 kJ per mole of formed CO_2 (DME) versus 803 kJ per mole of formed CO_2 (CH_4), respectively [95].

The specific feedstock demand of the SDR is 79 % higher than that of the SMR, primarily due to the 73 % higher LHV of methane compared to DME. This indicates that significantly larger feedstock masses are required when using DME, a general limitation of DME as a hydrogen carrier rather than a plant-specific issue. The SDR achieves a higher hydrogen yield than the SMR, despite its lower cold gas efficiency, owing to differences in the LHVs, the molar masses, and the stoichiometric coefficients. In terms of specific energy demand, the SMR performs only marginally better, requiring around 3 % less energy per kilogram of hydrogen. Overall, despite its higher feedstock demand, slightly lower efficiency, and marginally higher uncaptured emissions, the SDR remains a viable option for hydrogen production from rDME, offering the advantage of near-term applicability.

Table 3
Calculated efficiency parameters of the SDR and the SMR compared to literature values.

Parameters	This work		Literature
	SMR	SDR	SMR [94]
CGE / %	73.0	70.9	69.1
UCE / kg_{CO_2}/kg_{H_2}	1.03	1.12	0.99
UCE from RG / %	14.0	–	–
$m_{spec,feedstock}/kg_{feedstock}/kg_{H_2}$	3.28	5.87	3.73
Y_{H_2} / %	60.6	64.9	–
E_{H_2} / kWh/kg_{H_2}	45.8	47.2	48.2

3.2. Equipment sizing

The subsequent analysis evaluates the technical viability of transitioning from CH_4 as a feedstock to DME, utilizing the same equipment. To this end, an analysis is conducted of the transferred thermal energies in the heat exchangers and the electrical power consumptions of both setups (Fig. 6) to obtain a basic understanding of the sizes of the units, since both processes are very similar. The heat exchangers are grouped into categories (Table 4), and the efficiencies of the components are given in Table 5. The power demand of the air coolers is fixed at 2 % of their duty.

As demonstrated in Fig. 6, the total transferred thermal energy of the two processes is comparable, with values of 715 MW for the SMR and 684 MW for the SDR. The deviations in thermal energy between the SMR and the SDR are most significant in the hotbox, the air preheater, and the low-pressure steam system with the amine scrubber reboiler.

The heat demand for the reaction transferred in the SDR's hotbox is 69 % of that in the SMR's hotbox, owing to the lower endothermic nature of steam reforming of DME (R01) relative to that of CH_4 (R06). Consequently, less heat is required.

The air preheater of the SDR exhibits a 52 % reduction in heat exchange, attributable to its lower preheating temperature. This is primarily due to the SDR's elevated steam demand for the amine scrubber reboiler, resulting in a reduced energy availability for air preheating.

The transferred heat in the low-pressure steam system of the SDR is 40 % higher than for the SMR. The elevated steam demand of the SDR is attributable to the necessity of steam for the DME evaporator and the augmented energy demand of the amine scrubber reboiler. It has been shown that the SDR results in a greater overall production of CO_2, necessitating the capture of a greater volume of CO_2.

The higher CO content in the reformer outlet of the SDR results in a 59 % increase in thermal energy recovery through steam generation in the WGS reactor compared to the SMR's WGS reactor.

The overall required power (excluding the amine scrubber) of both processes is comparable with 3.35 MW for the SMR and 3.34 MW for the SDR (Fig. 6); however, the shares of the specific plant components differ. The most significant disparity arises from the flue gas blower, as the SMR requires approximately 0.1 MW more power due to its higher flue gas mass flow. This discrepancy can be attributed to the higher oxygen demand of the SMR's burner, which consequently leads to a significantly higher nitrogen mass flow in the flue gas. The DME educt pump requires 17 % more power than the pump for liquefied methane because the mass flow of DME is 62 % higher than that of methane. However, given the inherent differences in the feedstock, the necessity for distinct equipment remains unaltered.

The feasibility of directly retrofitting an SMR to DME remains uncertain due to discrepancies in the detailed plant design. The viability of this process depends on the particular design of the SMR, necessitating a comprehensive equipment study to ascertain the technical feasibility.

3.3. Parameter variation

In order to identify the parameters that will enable future process optimization, a parameter variation was conducted. The variation was applied to the following key process parameters: the reformer outlet temperature (T_{outlet}), the MT water-gas shift temperature (T_{MTWGS}), the steam-to-carbon ratio (S/C_{norm}), the H_2 recovery rate of the PSA, the amine scrubber reboiler duty per tonne of CO_2, and the amine scrubber's capture rate. The outcomes of this study are presented in Fig. 7. The results for the UCE are shown in Fig. 8. The reference values are indicated by a dotted line. The superheater and steam superheater are excluded from the analysis because the temperature variations in the steam superheater (HX09) and the superheater (HX03) had no numerical impact on the CGEs or the UCE. Therefore, the data are not shown in Figs. 7 and 8. The alterations in the steam superheater's temperature are counterbalanced by the superheater, whose duty is inversely adjusted to

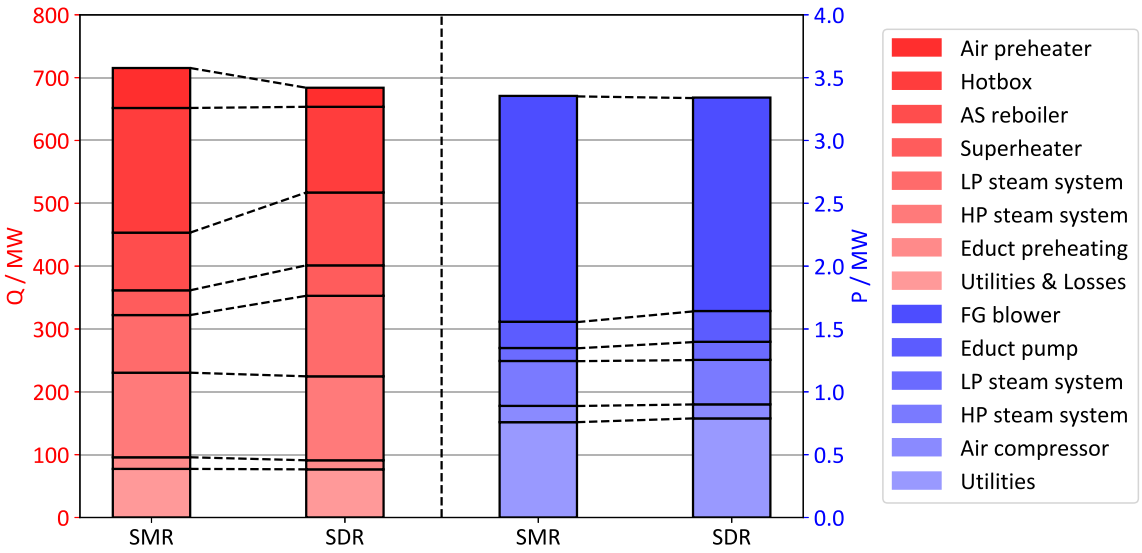

Fig. 6. Overview of the transferred thermal energies (Q) of heat exchangers (red) and power (P) consumption of electrical units (blue) from the SMR and the SDR.

Table 4
Heat exchange categories.

Categories	Heat exchangers
Hotbox	HX08
Air preheater	HX10
AS reboiler	HX13
LP steam system	HX05, HX11, HX12
Superheater	HX03
Educt preheating	HX01, HX02
HP steam system	HX04, HX06, HX07, HX09
Utilities & Losses	AC1, AC2, WC1, WC2, HL1, HL2, AH1

Table 5
Component efficiencies.

Efficiency (η)	Value
Electrical η of pumps and compressors	0.90 [97]
Adiabatic η (η_{adia}) of the pumps	0.50 [97]
η_{adia} of the flue gas blower	0.82 [98]
η_{adia} of the regasification blower	0.77 [98]
η_{adia} of the air compressor	0.82 [98]

maintain equilibrium, resulting in merely a redistribution of transferred thermal energies. A reduction in the superheater temperature facilitates enhanced air preheating, consequently elevating the burner temperature and augmenting heat transfer to the reformer. This increase in thermal energy is proportional to the reduction in the superheater's duty. Consequently, the alterations in both units (superheater and steam superheater) are counterbalanced by other components within the plant.

3.3.1. *Effect of the parameter variation on the CGE*

As demonstrated in Fig. 7A, the variation in the reformer outlet temperature indicates that an increase from 870 to 930 °C results in a 0.3 % CGE increase for the SMR and a 0.5 % CGE increase for the SDR. This is attributable to a reduced methane slip at higher temperatures. While the impact on the SDR is more pronounced, the overall impact is negligible.

In a similar manner, an increase in the water-gas shift temperature (Fig. 7B) from 220 to 320 °C results in an elevated CO slip (SE5). The additional CO is combusted in the hot box, thereby reducing the requirement for make-up fuel. While a higher CO slip results in a decrease in hydrogen content, this effect is less pronounced, and the CGE exhibits a slight improvement, ranging from 72.8 to 73.1 % (SMR) and from 70.6 to 71.0 % (SDR). As the CGE increases, the CGE-difference between the SMR and the SDR narrows. Consequently, elevated WGS temperatures could potentially amplify the CGE, suggesting a possible benefit from a high-temperature WGS reactor.

The CH_4 and CO slip are both influenced by the S/C_{norm} variations (Fig. 7C). While an increase in S/C_{norm} reduces the methane slip, thereby improving the CGE, it at the same time decreases the CO slip, exerting a negative effect on the CGE. The net effect of these opposing effects is that minimum CGEs of 72.94 % (SMR) and 70.85 % (SDR) occur at normalized S/Cs between 1.1 and 1.2, respectively, and CGE maxima at an S/C_{norm} of 1.1. Given the elevated risk of coking at a low S/C_{norm}, operating at a higher S/C_{norm} would be advantageous in this instance, particularly for the SMR. This is attributable to the fact that the impact of S/C_{norm} on the CGE is more pronounced for the SDR than for the SMR.

The absolute CGE difference between maximum and minimum is only 0.09 % for the SMR and 0.37 % for the SDR. Consequently, there is a possibility for the SDR to operate at low a S/C_{norm}; however, further experimental analysis is necessary to investigate the coking behavior.

While the impact of S/C_{norm} and the temperatures is only minor within the analyzed range, the hydrogen recovery rate of the PSA (Fig. 7D) has a greater impact on the CGEs of the SMR and the SDR. An enhancement in the recovery rate leads to an improvement in the CGEs, owing to the enhanced efficiency in utilizing a portion of the feed as fuel in lieu of a portion of the H_2 product. By increasing the recovery rate from 82 to 92 %, the CGEs exhibit an increase from 72.3 to 73.6 % (SMR) and from 70.2 to 71.5 % (SDR). Consequently, a well-performing PSA unit is crucial for both the SMR and the SDR.

The amine scrubber reboiler duty exerts a substantial influence on the CGE (Fig. 7E), leading to a reduction in efficiency by 7.2 % for the SDR and 5.8 % for the SMR when the duty is elevated from 1.8 to 2.8 GJ per tonne of CO_2. As the reboiler duty increases, the CGE gap between the SMR and the SDR widens. While the optimization of the reboiler duty is imperative for both systems, the SDR has the potential to further reduce the CGE gap to the SMR by enhancing the performance of the amine scrubber. Consequently, in the context of DME steam reforming, enhancing carbon capture emerges as a pivotal concern.

The impact of varying the capture rate between 85 and 95 % (Fig. 7F) on the CGE is analogous to the impact of the PSA recovery rate. An increase in the carbon capture rate from 85 to 95 % results in a reduction of the CGE from 73.5 to 72.4 % (SMR) and from 71.6 to 70.2 % (SDR), with the SDR exhibiting a more pronounced decrease due to a higher CO_2 mass flow in the flue gas. While an augmented capture rate is advantageous for the DME/CO_2-cycle, it at the same time reduces

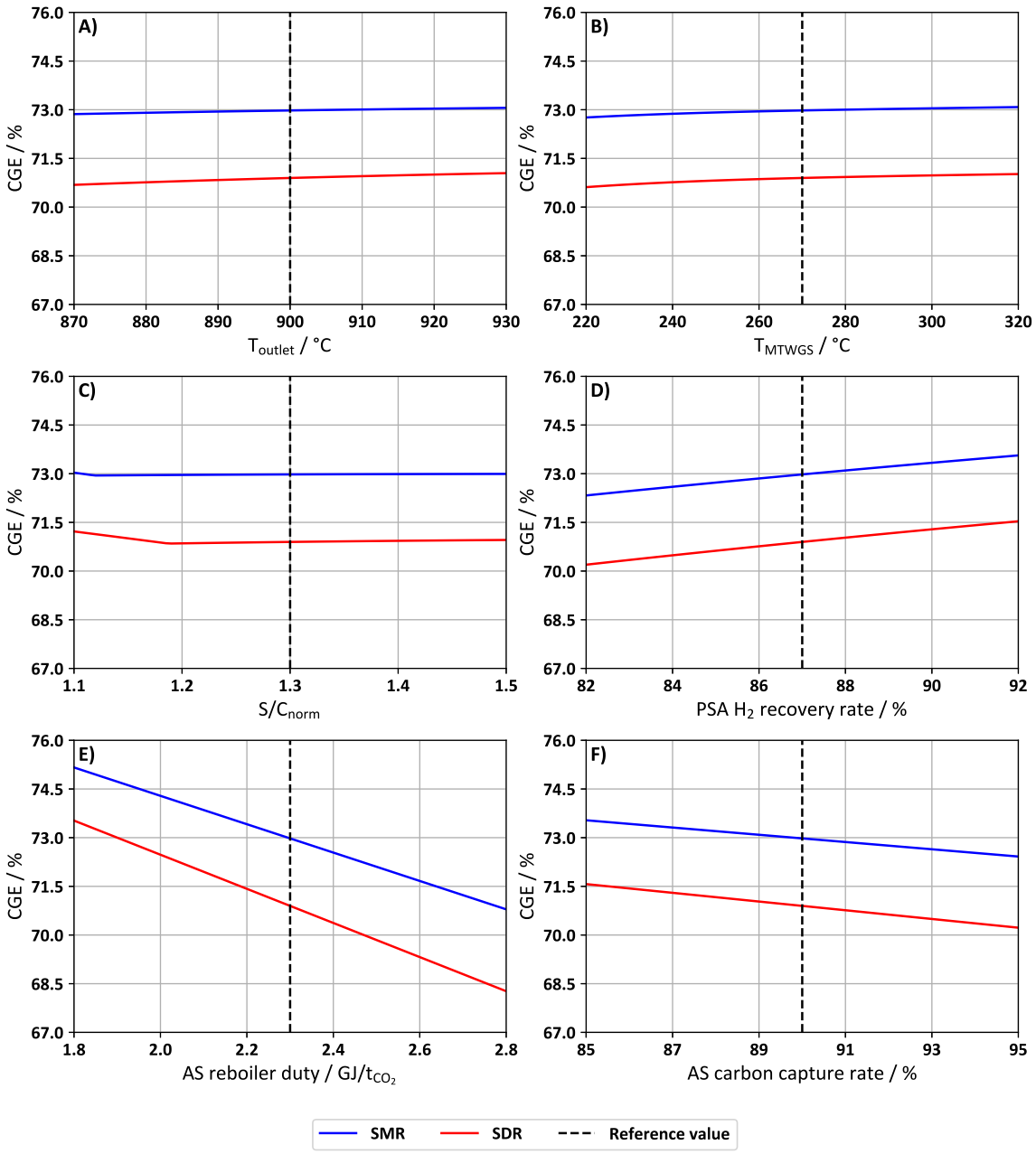

Fig. 7. Influence of the variation of the process variables: A) reformer outlet temperature, B) MT-WGS temperature, C) S/C_{norm}, D) PSA H_2 recovery rate, E) reboiler duty of the amine scrubber and F) amine scrubber capture rate on the CGEs of the SMR and SDR.

efficiency and likely increases the reboiler duty of the amine scrubber, further reducing the CGE.

3.3.2. *Effect of the parameter variation on* $m_{spec,feedstock}$ *and* Y_{H_2}

Both $m_{spec,feedstock}$ and Y_{H_2} are closely linked to the CGE. Fig. 8 illustrates these correlations: while the hydrogen yield exhibits a linear dependency on the CGE, the specific feedstock demand displays an inverse dependence.

Across all parameter ranges, the hydrogen yield is consistently higher for the SDR than for the SMR, with an average difference of around 4.5 percentage points. For PSA recovery and capture rate, this difference widens at higher settings, while it narrows with increasing reboiler duty. This advantage stems from DME's lower reaction enthalpy (20.4 vs. 41.2 kJ/mol H_2), though it is partly offset by higher CO_2 generation per mole of hydrogen (0.33 vs. 0.25).

In contrast, the specific feedstock demand shows only minor variations for most parameters (<2 %), with changes of about ±1.5–2 % for PSA recovery and capture rate. The reboiler duty exerts the strongest influence: increasing it from 1.8 to 2.8 GJ per tonnne CO_2 raises the feedstock demand by 6.2 % for SMR (3.19 to 3.39 kg_{CH_4}/kg_{H_2}) and 7.7 % for SDR (5.66 to 6.09 kg_{DME}/kg_{H_2}). Detailed graphs illustrating these parameter trends are provided in the Supplementary Information (Figs. S1 and S2).

3.3.3. *Effect of the parameter variation on the UCE*

As demonstrated in Fig. 9, the UCE generally exhibits opposing trends to the CGE and are proportional to the absolute captured CO_2, with the exception of emissions from the regasifier flue gas. An increase in captured CO_2 has been shown to result in a rise in low-pressure steam demand, thereby reducing the CGE as the energy cannot be recovered within the system. Consequently, these trends can be attributed to the same underlying mechanisms, as discussed for the CGE.

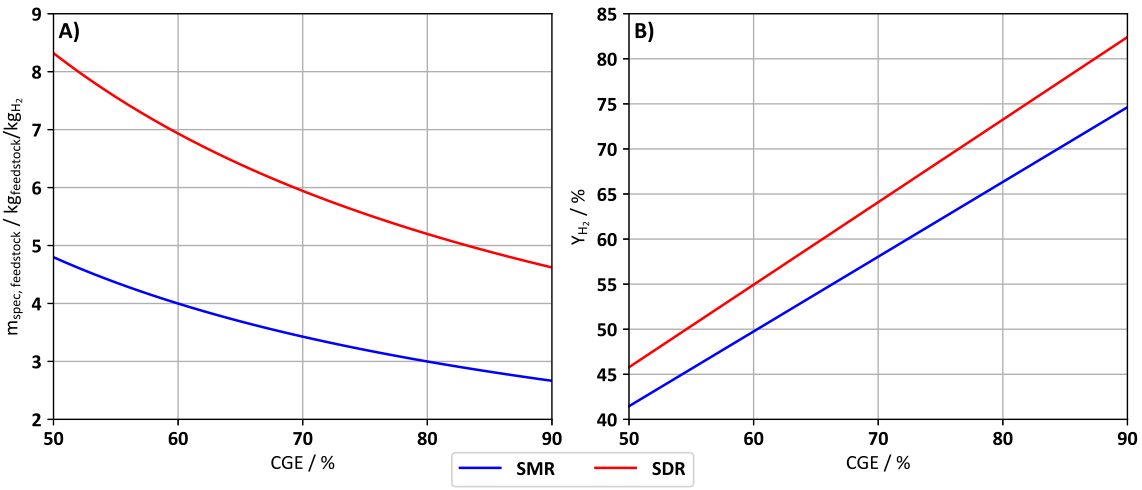

Fig. 8. Correlations between the CGE and the process parameters: A) hydrogen yield (Y_{H2}) and B) specific feedstock demand ($m_{spec,feedstock}$).

Increasing the reformer outlet temperature from 870 to 930 °C (Fig. 9A) results in a decrease in the UCE by 0.3 % (SMR) and 0.5 % (SDR). A comparable impact is observed with the MT-WGS reactor temperature (Fig. 9B): an increase from 220 to 320 °C results in a decrease of 0.3 % (SMR) and 0.4 % (SDR) in UCE.

For the variation of S/C_{norm} (Fig. 9C) the UCE have a maximum between 1.1 and 1.2. For the SMR 1.033 kg_{CO_2}/kg_{H_2} and for the SDR 1.122 kg_{CO_2}/kg_{H_2}. The lowest UCE are for S/C_{norm} of 1.1, with a minimum of 1.032 kg_{CO_2}/kg_{H_2} for the SMR and 1.116 kg_{CO_2}/kg_{H_2} for the SDR. This represents a decrease of only 0.12 % for the SMR and 0.53 % for the SDR. Similarly, by increasing the PSA hydrogen recovery rate (Fig. 9D) from 82 to 92 % the UCE decrease from 1.04 to 1.02 kg_{CO_2}/kg_{H_2} for the SMR and from 1.13 to 1.11 kg_{CO_2}/kg_{H_2} for the SDR. This represents a decrease of 1.68 % for the SMR and 1.87 % for the SDR. The variation of the amine scrubber reboiler duty from 1.8 to 2.8 GJ per tonne of CO_2 (Fig. 9E) leads to UCE increases of 6.2 % (SMR) and 7.2 % (SDR). As for the CGEs, the improvement in the amine scrubber has a greater impact on the SDR than on the SMR.

The variation in capture rates is predominantly responsible for the distinction in trends observed between Fig. 9 and Fig. 7. An increase in the carbon capture rate corresponds to a decline in both the CGE and the UCE, with the SDR curve exhibiting a steeper gradient in both instances. While the disparity in the CGE increases with elevated carbon capture rates, the UCE discrepancy diminishes until both curves intersect at approximately 93.8 % carbon capture rate. This outcome is attributable to the LNG regasifier, wherein flue gas CO_2 is not captured. It is noteworthy that augmenting the carbon capture rate from 90 to 95 % results in a mere 43 % reduction in UCE for the SMR and approximately 50 % for the SDR.

Within the range that was analyzed, the variations of the reformer outlet temperature, the MT-WGS temperature, and S/C_{norm} have an impact of less than 1 % on UCE. The PSA hydrogen recovery rate has been shown to have a moderate impact of approximately 1.8 %, with a higher recovery rate resulting in a reduction in UCE. Given the constant hydrogen production rate, a reduced PSA recovery necessitates an augmented carbon feedstock to counterbalance the diminished hydrogen production.

The amine scrubber reboiler duty variation demonstrates significant disparities, with an SDR discrepancy of 7.2 % and an SMR discrepancy of 6.2 % between minimum and maximum. Increases in reboiler duties necessitate greater steam production, resulting in the utilization of additional feedstock as fuel, which in turn leads to elevated CO_2 emissions. For the UCE, as for the CGE, the capture rate has the most significant influence. For the SMR, changes of approximately ±42 % to the reference value are observed, while for the SDR, the changes are approximately ±49 %.

Therefore, the amine scrubber is the pivotal unit that exerts a significant influence on the UCE. As shown above, in context of the DME/CO_2 cycle CO_2 has to be captured either at the reformer or via direct air capture whereby capturing at the reformer is economically beneficial. It is therefore desirable to reduce the amine scrubber's reboiler duty while maintaining the carbon capture rate as high as possible.

3.3.4. *Effect of the parameter variation on* E_{H_2}

The specific energy demand for hydrogen, E_{H_2}, is determined by the specific feedstock requirement ($m_{spec,feedstock}$; see also Fig. S2 in the supplementary information) and the overall plant electricity demand (see also Fig. S3 in the supplementary information). Since electricity energy accounts for only about 0.4 % of the total energy, its influence is negligible. Fig. 9 illustrates the parameter variation for E_{H_2}. In contrast to the CGE, the trends are reversed: the SMR requires between 44.5 and 47.5 kWh/kg_{H_2}, while the SDR lies between 45.5 and 49.0 kWh/kg_{H_2}.

The effects of the reformer outlet and WGS temperature are negligible, as the variations in E_{H_2} remain below 1 % in both cases. For the outlet temperature (Fig. 9A), the SMR decreases by only 0.3 % (from 45.91 to 45.79 kWh/kg_{H_2}) and the SDR by 0.5 % (from 47.33 to 47.08 kWh/kg_{H_2}). A similar trend is observed for the WGS temperature (Fig. 9B), with decreases of 0.4 % for the SMR (from 45.98 to 45.78 kWh/kg_{H_2}) and 0.6 % for the SDR (from 47.37 to 47.10 kWh/kg_{H_2}).

For the normalized steam-to-carbon ratio (S/C_{norm}, Fig. 9C), E_{H_2} follows the same trend as the UCE, with a flat maximum at 1.12 (SMR) and 1.19 (SDR). The difference between maximum and minimum values is only 0.06 kWh/kg_{H_2} for the SMR (from 45.86 to 45.80 kWh/kg_{H_2}) and 0.25 kWh/kg_{H_2} for the SDR (from 47.21 to 46.96 kWh/kg_{H_2}), corresponding to relative changes below 1 % in both cases.

The PSA hydrogen recovery and AS CO_2 capture rates (Fig. 9D and F) have a slightly larger effect. With increasing PSA recovery, E_{H_2} decreases by 1.7 % for the SMR (from 46.26 to 45.47 kWh/kg_{H_2}) and by 1.9 % for the SDR (from 47.66 to 46.75 kWh/kg_{H_2}). Conversely, increasing the capture rate raises E_{H_2} by 1.5 % in the SMR (from 45.49 to 46.20 kWh/kg_{H_2}) and by 1.9 % in the SDR (from 46.74 to 47.63 kWh/kg_{H_2}).

The strongest sensitivity is observed for the AS reboiler duty (Fig. 9E). Here, the SMR energy demand increases by 6.2 % (from 44.50 to 47.26 kWh/kg_{H_2}), and the SDR by 7.7 % (from 45.49 to 49.00 kWh/kg_{H_2}).

Overall, the relative changes in E_{H_2} closely mirror those of $m_{spec,feedstock}$, since more than 99 % of the energy originates from the feedstock. This highlights that plant-wide electrical optimization plays only a minor role compared to improvements in the utilization of the feedstock's chemical energy (Fig. 10).

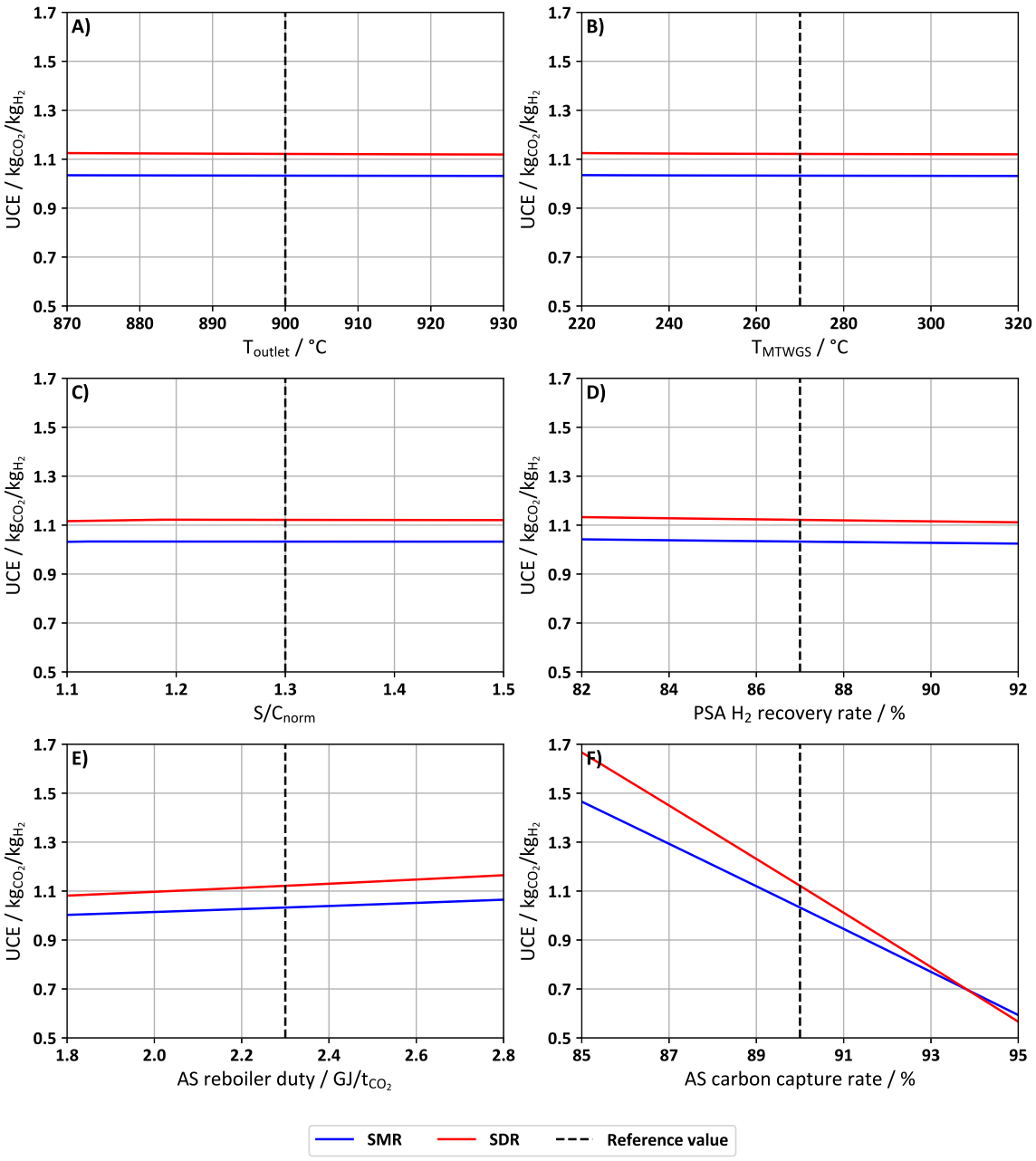

Fig. 9. Influence of the variation of the process variables: A) reformer outlet temperature, B) MT-WGS temperature, C) S/C$_{norm}$, D) PSA H_2 recovery rate, E) reboiler duty of the amine scrubber, F) amine scrubber capture rate on the UCE of the SMR and SDR.

3.3.5. *CO_2 in DME feed*

A final analysis was conducted to determine the impact of the CO_2 content in the DME feed on the performance of the SDR. Given that both DME and CO_2 are transported in the same vessel within the DME/CO_2-cycle, it is probable that low CO_2 concentrations are present in the DME. To this end, a simulation was conducted in which the CO_2 content in the feed ranged from 0 to 15 mol%. All other parameters remain at their reference values, as established in the simulation methodology. The impact on the CGE and UCE is illustrated in Fig. 11.

While the CGE decreases with increasing CO_2 content, the UCE increase. The CGE decreases by 1.9 % (from 70.9 to 69.5 %) as CO_2 content increases from 0 to 15 %. Meanwhile, the UCE increase by 11.0 % (from 1.12 to 1.24 kg$_{CO_2}$/kg$_{H_2}$) over the same range. While the decrease in the CGE is manageable, the significant increase in UCE is challenging. This is because the uncaptured CO_2 cannot be back-shipped, and instead must be removed from the atmosphere by CO_2 removal to close the carbon loop.

4. Conclusion & outlook

In this simulation study it has been shown that the adaptation of the state-of-the-art steam methane reforming to renewable dimethyl ether as a feedstock has potential to substantially enhance the technology readiness level of the DME steam reforming process. This in turn enables the DME/CO_2-cycle and the utilization of DME as a renewable hydrogen carrier.

A comparison of DME to conventional CH_4 steam reforming reveals that the SDR exhibits marginally reduced performance relative to the SMR with respect to cold gas efficiency (70.9 vs. 73.0 %), specific feedstock demand (5.87 vs. 3.28 kg$_{feedstock}$/kg$_{H_2}$), specific energy demand per hydrogen (47.2 vs. 45.8 kWh/kg$_{H_2}$) and uncaptured CO_2 emissions (1.12 vs. 1.03 kg$_{CO_2}$/kg$_{H_2}$). Its clear advantage lies in the higher

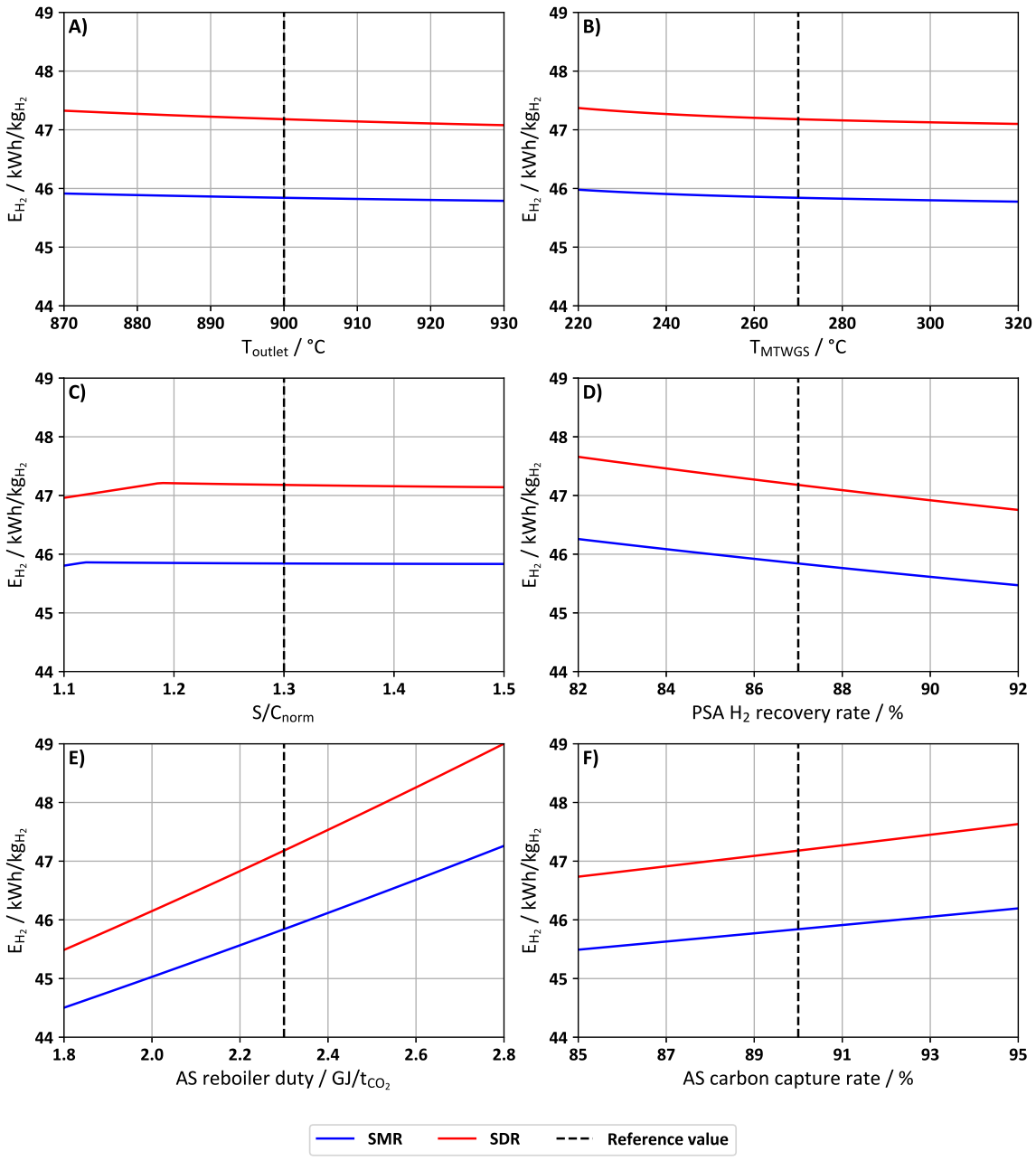

Fig. 10. Influence of the variation of the process variables: A) reformer outlet temperature, B) MT-WGS temperature, C) S/C_{norm}, D) PSA H_2 recovery rate, E) reboiler duty of the amine scrubber and F) amine scrubber capture rate on E_{H2} of the SMR and SDR.

hydrogen yield (64.9 % vs. 60.6 %). The disparities observed are uncritical so that DME can be considered a viable alternative, particularly given its potential role in renewable hydrogen pathways. Both reforming routes can be further optimized, which lies beyond the scope of this study but is well documented in the literature [99,100].

In order to adequately assess the overall suitability of DME as a hydrogen carrier in comparison to CH_4, it is imperative to consider factors beyond the mere reforming step. Achieving higher efficiencies in other parts of the DME/CO_2-cycle can lead to DME outperforming CH_4. For instance, the liquefaction of CH_4 is more energy intensive than the liquefaction of DME, and the transport of DME is more efficient.

However, the amine scrubber's performance has the most significant impact on cold gas efficiency and uncaptured carbon emissions. The results suggest that improving the capture rate and reducing the reboiler duty will improve the SDR's competitiveness with the SMR. Therefore, optimizing the amine scrubber efficiency is a key focus for future research. In this context, achieving the highest feasible capture rate while maintaining efficiency is critical. At the same time, improvements in carbon capture from the atmosphere, such as direct air capture (DAC), would enhance the competitiveness of all carbon-based hydrogen carriers. However, given the maturity gap between DAC and amine scrubbing, near-term deployment of renewable DME reforming requires integration with high-efficiency capture at the reformer site. For this reason, current systems must rely on high-efficiency amine-based capture, while future advances in DAC may provide complementary options once the technology becomes more energy-efficient and commercially viable.

Experimental studies are required to validate DME steam reforming at elevated temperatures, with a particular focus on coking behavior and the reaction mechanism, in comparison to CH_4 steam reforming. A critical question to be addressed in future research is the comparison of catalyst longevity between these two reactions. Furthermore, additional

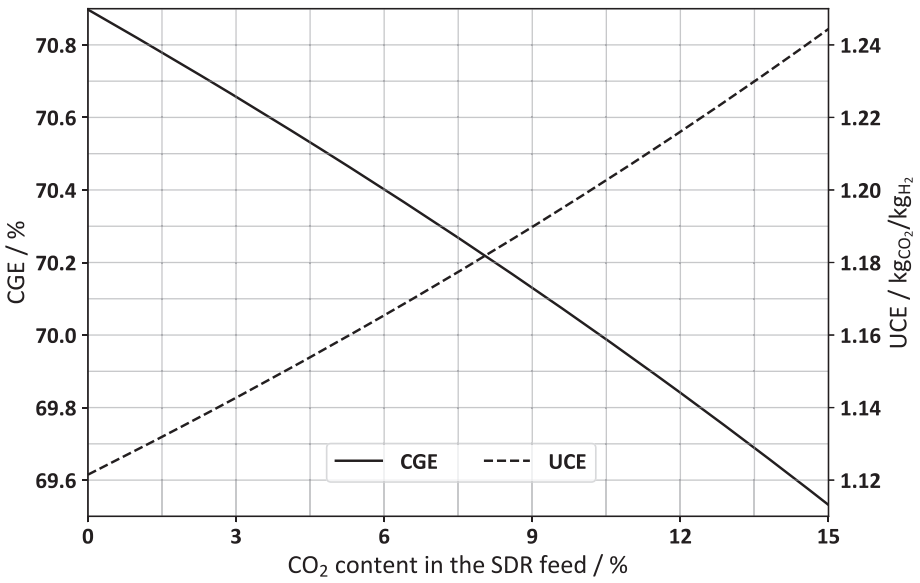

Fig. 11. Effect of CO_2 content in the SDR feed on the CGE and the UCE.

studies are necessary to ascertain whether the revamp of an existing SMR plant to DME is a viable option, as a newly designed plant for DME steam reforming appears to be a feasible proposition. However, it is imperative to emphasize the necessity of conducting detailed design studies for critical equipment to ensure the optimal performance of the plant.

In addition, the performance of a low-temperature DME steam reformer in comparison to the results of this study should be investigated in future simulation studies. Another promising approach involves the implementation of an autothermal reformer (ATR) [63] for DME reforming. Additionally, the ongoing investigations into electrically heated reformers (e-SMR) could prove to be of interest in the context of DME steam reforming [101]. Both ATR and e-SMR have the potential to substantially decrease the effort required for CO_2 capture, making them a subject of considerable interest for further exploration. Investigating these pathways in parallel with high-temperature SDR will help identify the most practical trade-offs between efficiency, flexibility, and integration into renewable energy systems.

Furthermore, to comprehensively assess DME steam reforming within the broader context of the DME/CO_2-cycle, future studies must ascertain the extent of CO_2 content in DME. Additionally, a crucial element for future studies is the evaluation of a higher amine scrubber capture rate versus direct air capture. Subsequent studies should also assess additional carbon capture options [89,90,102]. Complementary life-cycle analyses and cost studies are also needed to establish both the environmental and economic viability of DME as a hydrogen carrier.

CRediT authorship contribution statement

Timm Ruther: Writing – original draft, Visualization, Methodology, Investigation, Conceptualization. **Hannes Stadler:** Writing – review & editing, Visualization, Supervision, Conceptualization. **Andreas Peschel:** Writing – review & editing, Supervision, Project administration, Methodology, Conceptualization.

Declaration of Generative AI and AI-assisted technologies in the writing process

During the preparation of this work, the authors used GPT-4o from OpenAI and DeepL Write from DeepL SE to improve the quality of the writing in terms of grammatical correctness and style. After using these tools, the authors reviewed and edited the content as needed and take full responsibility for the published article.

Declaration of competing interest

Forschungszentrum Jülich GmbH and Andreas Peschel have a patent application related to the high-temperature steam reforming of dimethyl ether. Timm Ruther, Hannes Stadler, and Andreas Peschel are employees of Forschungszentrum Jülich GmbH.

Acknowledgments

The authors acknowledge the funding by the German Federal Ministry of Research, Technology and Space and the Ministry of Economic Affairs, Industry, Climate Action and Energy of the State of North Rhine-Westphalia through the project HC-H2.

Appendix A. Supplementary data

Supplementary data to this article can be found online at https://doi.org/10.1016/j.cej.2025.168929.

Data availability

The authors declare that the data supporting the findings of this study are available within the paper and its Supplementary Information.

References

[1] IRENA, Geopolitics of the Energy Transformation: The Hydrogen Factor. https://www.irena.org/Digital-Report/Geopolitics-of-the-Energy-Transformation. (Accessed 13 February 2025).
[2] R. Rikabi, Green Hydrogen Imports into Europe: An Assessment of Potential Sources. https://www.oxfordenergy.org/wpcms/wp-content/uploads/2024/04/ET32-Green-Hydrogen-Imports-into-Europe-An-Assessment-of-Potential-Sources.pdf, 2024. (Accessed 9 January 2025).
[3] A. Peschel, Industrial perspective on hydrogen purification, compression, storage, and distribution, Fuel Cells 20 (2020) 385–393, https://doi.org/10.1002/fuce.201900235.
[4] European Commission, Assessment of Hydrogen Delivery Options. https://joint-research-centre.ec.europa.eu/document/download/5cdbd6f7-7ab4-447b-be0a-dde0a25198ab_en, 2021. (Accessed 9 January 2025).
[5] U.S. DRIVE, Hydrogen Delivery Technical Team, Roadmap. https://www.osti.gov/servlets/purl/1220133, 2013. (Accessed 6 March 2025).
[6] J.D. Hunt, P.M. Montanari, D.N. Hummes, M. Taghavi, B. Zakeri, O.J. Romero, W. Zhou, M.A.V. de Freitas, N. José de Castro, P.S. Schneider, Y. Wada, Solid air hydrogen liquefaction, the missing link of the hydrogen economy, Int. J. Hydrog.

Energy 48 (2023) 29198–29208, https://doi.org/10.1016/j.ijhydene.2023.03.405.
[7] M. Weikl, A. Peschel, Industrial view on hydrogen carriers for intercontinental transport, Curr. Opin. Green Sustain. Chem 44 (2023) 100843, https://doi.org/10.1016/j.cogsc.2023.100843.
[8] P. Schühle, R. Stöber, M. Semmel, A. Schaadt, R. Szolak, S. Thill, M. Alders, C. Hebling, P. Wasserscheid, O. Salem, Dimethyl ether/CO2 – a hitherto underestimated H2 storage cycle, Energy Environ. Sci. (2023), https://doi.org/10.1039/D3EE00228D.
[9] R. Anggarani, C.S. Wibowo, D. Rulianto, Application of dimethyl ether as LPG substitution for household stove, Energy Procedia 47 (2014) 227–234, https://doi.org/10.1016/j.egypro.2014.01.218.
[10] WLGA, Renewable DME in the LPG Industry, UN Approval of 12% DME/LPG Drop-in Blend. https://www.worldliquidgas.org/news/renewable-dme-in-the-lpg-industry-un-approval-of-12-dme-lpg-drop-in-blend/. (Accessed 21 February 2025).
[11] U.S. Department of Energy, Dimethyl Ether. https://afdc.energy.gov/fuels/emerging-dme. (Accessed 3 January 2025).
[12] Methanol Institute, DME: An Emerging Global Fuel. https://www.methanol.org/wp-content/uploads/2016/06/DME-An-Emerging-Global-Guel-FS.pdf. (Accessed 21 February 2025).
[13] S. Lee, M. Gogate, C.J. Kulik, Methanol-to-gasoline vs. DME-to-gasolne II. Process comparison and analysis, Fuel Sci. Technol. Int. 13 (1995) 1039–1057, https://doi.org/10.1080/08843759508947721.
[14] Johnson Matthey, Dimethyl Ether Production: Replace LPG With Sustainable Dimethyl Ether Using Johnson Matthey's Production Technology, in: https://matthey.com/products-and-markets/chemicals/process-licensing/dimethyl-ether-production. (Accessed 21 February 2025).
[15] Science Japan, Using Low-temperature, Low-pressure Liquefied CO2 to Realize Low-cost Mass Transportation: Demonstration Test Ship "EXCOOL" Completed With Expectations for Social Implementation in the Future. https://sj.jst.go.jp/news/202401/n0115-02k.html. (Accessed 10 February 2025).
[16] Mitsubishi Shipbuilding Co, Liquefied CO2 Carrier "EXCOOL", Mitsubishi Heavy Industries Technical Review 61. https://www.mhi.co.jp/technology/review/pdf/e612/e612050.pdf, 2024. (Accessed 28 April 2025).
[17] N. Laosiripojana, S. Assabumrungrat, Catalytic steam reforming of dimethyl ether (DME) over high surface area Ce–ZrO2 at SOFC temperature: the possible use of DME in indirect internal reforming operation (IIR-SOFC), Appl. Catal. A Gen. 320 (2007) 105–113, https://doi.org/10.1016/j.apcata.2006.12.018.
[18] V.A. Sobyanin, S. Cavallaro, S. Freni, Dimethyl ether steam reforming to feed molten carbonate fuel cells (MCFCs), Energy Fuel 14 (2000) 1139–1142, https://doi.org/10.1021/ef990201s.
[19] T.A. Semelsberger, R.L. Borup, Thermodynamics of Hydrogen Production from Dimethyl Ether Steam Reforming and Hydrolysis. https://www.osti.gov/servlets/purl/836682, 2004. (Accessed 6 March 2025).
[20] K. Faungnawakij, R. Kikuchi, K. Eguchi, Thermodynamic analysis of carbon formation boundary and reforming performance for steam reforming of dimethyl ether, J. Power Sources 164 (2007) 73–79, https://doi.org/10.1016/j.jpowsour.2006.09.072.
[21] J.O. Ighalo, A.G. Adeniyi, Thermodynamic modelling of dimethyl ether steam reforming, Clean Techn. Environ. Policy 23 (2021) 1353–1363, https://doi.org/10.1007/s10098-021-02033-y.
[22] P. Bipinkumar (Oberon Fuels) U.S. Patent 2024/0109773 A1, 2024.
[23] R. Stöber, F. Seidl, E. Hoffmann, P. Wasserscheid, P. Schühle, A highly durable catalyst system for hydrogen production from dimethyl ether, Sustain. Energy Fuels 8 (2024) 1740–1749, https://doi.org/10.1039/D4SE00059E.
[24] S.S. Rahatade, N.A. Mali, Techno-economic assessment of hydrogen production via dimethylether steam reforming and methanol steam reforming, Indian Chem. Eng. 65 (2023) 352–368, https://doi.org/10.1080/00194506.2022.2162450.
[25] J. Hine, K. Arata, Keto-enol tautomerism. II. The calorimetrical determination of the equilibrium constants for keto-enol tautomerism for cyclohexanone and acetone, Bull. Chem. Soc. Jpn. 49 (1976) 3089–3092, https://doi.org/10.1246/bcsj.49.3089.
[26] J.A. Manion, Evaluated enthalpies of formation of the stable closed shell C1 and C2 chlorinated hydrocarbons, J. Phys. Chem. Ref. Data Monogr. 31 (2002) 123–172, https://doi.org/10.1063/1.1420703.
[27] National Institute of Standards and Technology, NIST-JANAF Thermochemical Tables - SRD 13: Carbon Dioxide (CO2). https://janaf.nist.gov/tables/C-095.html. (Accessed 25 February 2025).
[28] National Institute of Standards and Technology, NIST-JANAF Thermochemical Tables - SRD 13: Water (H2O). https://janaf.nist.gov/tables/H-064.html. (Accessed 25 February 2025).
[29] National Institute of Standards and Technology, NIST-JANAF Thermochemical Tables - SRD 13: Carbon Monoxide (CO). https://janaf.nist.gov/tables/C-093.html. (Accessed 25 February 2025).
[30] G. Pilcher, A.S. Pell, D.J. Coleman, Measurements of heats of combustion by flame calorimetry. Part 2.—dimethyl ether, methyl ethyl ether, methyl n-propyl ether, methyl isopropyl ether, Trans. Faraday Soc. 60 (1964) 499–505, https://doi.org/10.1039/TF9646000499.
[31] National Institute of Standards and Technology, NIST-JANAF Thermochemical Tables - SRD 13: Hydrogen (H2). https://janaf.nist.gov/tables/H-050.html. (Accessed 14 March 2025).
[32] E. Pawelczyk, N. Łukasik, I. Wysocka, A. Rogala, J. Gębicki, Recent progress on hydrogen storage and production using chemical hydrogen carriers, Energies 15 (2022) 4964, https://doi.org/10.3390/en15144964.
[33] D. Kim, G. Park, B. Choi, Y.-B. Kim, Reaction characteristics of dimethyl ether (DME) steam reforming catalysts for hydrogen production, Int. J. Hydrog. Energy 42 (2017) 29210–29221, https://doi.org/10.1016/j.ijhydene.2017.10.020.
[34] V. Galvita, G. Semin, V. Belyaev, T. Yurieva, V. Sobyanin, Production of hydrogen from dimethyl ether, Appl. Catal. A Gen. 216 (2001) 85–90, https://doi.org/10.1016/S0926-860X(01)00540-3.
[35] Z. Sun, Y. Tian, P. Zhang, G. Yang, N. Tsubaki, T. Abe, A. Taguchi, J. Zhang, L. Zheng, X. Li, Sputtered Cu-ZnO/γ-Al 2 O 3 bifunctional catalyst with ultra-low Cu content boosting dimethyl ether steam reforming and inhibiting side reactions, Ind. Eng. Chem. Res. 58 (2019) 7085–7093, https://doi.org/10.1021/acs.iecr.9b01214.
[36] K. Faungnawakij, K. Eguchi, Dimethyl ether—reforming catalysts for hydrogen production, Catal. Surv. Jpn. 15 (2011) 12–24, https://doi.org/10.1007/s10563-010-9103-7.
[37] K. Takeishi, Steam reforming of dimethyl ether, Appl. Catal. A Gen. 260 (2004) 111–117, https://doi.org/10.1016/j.apcata.2003.10.006.
[38] R. González-Gil, C. Herrera, M.Á. Larrubia, P. Kowalik, I.S. Pieta, L.J. Alemany, Hydrogen production by steam reforming of DME over Ni-based catalysts modified with vanadium, Int. J. Hydrog. Energy 41 (2016) 19781–19788, https://doi.org/10.1016/j.ijhydene.2016.05.074.
[39] J.-H. Lian, H.-Y. Tan, C.-Q. Guo, L.-S. Shen, Z.-X. Lu, Y. Shi, C.-F. Yan, Unravelling the role of ceria in improving the stability of Mo 2 C- based catalysts for the steam reforming of dimethyl ether, Catal. Sci. Technol. 11 (2021) 5570–5578, https://doi.org/10.1039/d1cy00824b.
[40] Y. Yamada, T. Mathew, A. Ueda, H. Shioyama, T. Kobayashi, A novel DME steam-reforming catalyst designed with fact database on-demand, Appl. Surf. Sci. 252 (2006) 2593–2597, https://doi.org/10.1016/j.apsusc.2005.05.087.
[41] M. Yang, Y. Men, S. Li, G. Chen, Hydrogen production by steam reforming of dimethyl ether over ZnO–Al2O3 bi-functional catalyst, Int. J. Hydrog. Energy 37 (2012) 8360–8369, https://doi.org/10.1016/j.ijhydene.2012.02.070.
[42] F. Fan, Q. Zhang, X. Wang, Y. Ni, Y. Wu, Z. Zhu, A structured Cu-based/γ-Al 2 O 3 /Al plate-type catalyst for steam reforming of dimethyl ether: Self-activation behavior investigation and stability improvement, Fuel 186 (2016) 11–19, https://doi.org/10.1016/j.fuel.2016.08.036.
[43] K. Faungnawakij, Y. Tanaka, N. Shimoda, T. Fukunaga, S. Kawashima, R. Kikuchi, K. Eguchi, Influence of solid–acid catalysts on steam reforming and hydrolysis of dimethyl ether for hydrogen production, Appl. Catal. A Gen. 304 (2006) 40–48, https://doi.org/10.1016/j.apcata.2006.02.021.
[44] J. Vicente, A.G. Gayubo, J. Ereña, A.T. Aguayo, M. Olazar, J. Bilbao, Improving the DME steam reforming catalyst by alkaline treatment of the HZSM-5 zeolite, Appl. Catal. B Environ. 130-131 (2013) 73–83, https://doi.org/10.1016/j.apcatb.2012.10.019.
[45] K. Faungnawakij, R. Kikuchi, T. Fukunaga, K. Eguchi, Stability enhancement in Ni-promoted Cu−Fe spinel catalysts for dimethyl ether steam reforming, J. Phys. Chem. C 113 (2009) 18455–18458, https://doi.org/10.1021/jp908365a.
[46] K. Faungnawakij, N. Shimoda, N. Viriya-empikul, R. Kikuchi, K. Eguchi, Limiting mechanisms in catalytic steam reforming of dimethyl ether, Appl. Catal. B Environ. 97 (2010) 21–27, https://doi.org/10.1016/j.apcatb.2010.03.010.
[47] K. Faungnawakij, T. Fukunaga, R. Kikuchi, K. Eguchi, Deactivation and regeneration behaviors of copper spinel–alumina composite catalysts in steam reforming of dimethyl ether, J. Catal. 256 (2008) 37–44, https://doi.org/10.1016/j.jcat.2008.02.022.
[48] M. Heidlage, R. Muralidharan, J. Tafoya, R.L. Borup, T.A. Semelsberger, DME as a Renewable Hydrogen Carrier: Innovative Approach to Renewable Hydrogen Production. https://www.hydrogen.energy.gov/docs/hydrogenprogramlibraries/pdfs/review23/st242_heidlage_2023_p-pdf.pdf, 2023. (Accessed 6 March 2025).
[49] S. Wei, C. Li, Design and optimization of spiral heated tubular dimethyl ether (DME) steam reforming reactor, Int. J. Hydrog. Energy 48 (2023) 2231–2246, https://doi.org/10.1016/j.ijhydene.2022.09.295.
[50] M. Hori, S. Shiozawa, Research and development for nuclear production of hydrogen in Japan, in: A. Terada, Y. Imai, H. Noguchi, H. Ota, A. Kanagawa, S. Ishikura, S. Kubo, J. Iwatsuki, K. Onuki, R. Hino (Eds.), Nuclear Production of Hydrogen, OECD, 2006, pp. 55–72.
[51] Haldor Topsøe, Hydrogen, methanol reforming, in: Hydrocarbon Processing (Ed.), Special Report: Gas Processing Developments: Gas Processes Handbook, 2006, p. 36.
[52] S. Hao, Y. Li, Y. Cheng, Z. Wang, Hydrogen production process based on methanol steam reforming, Fine Chemicals (1998) 52–54.
[53] F.A. Elewuwa, Y.T. Makkawi, Hydrogen production by steam reforming of DME in a large scale CFB reactor. Part I: Computational model and predictions, Int. J. Hydrog. Energy 40 (2015) 15865–15876, https://doi.org/10.1016/j.ijhydene.2015.10.050.
[54] F.A. Elewuwa, Y.T. Makkawi, A computational model of hydrogen production by steam reforming of dimethyl ether in a large scale CFB reactor. Part II: Parametric analysis, Int. J. Hydrog. Energy 41 (2016) 19819–19828, https://doi.org/10.1016/j.ijhydene.2016.08.072.
[55] C. Ledesma, E. López, T. Trifonov, Á. Rodríguez, J. Llorca, Catalytic reforming of dimethyl ether in microchannels, Catal. Today 323 (2019) 209–215, https://doi.org/10.1016/j.cattod.2018.03.011.
[56] M. Bianchini, N. Alayo, L. Soler, M. Salleras, L. Fonseca, J. Llorca, A. Tarancon, Standalone Micro-reformer for On-board Hydrogen Production From Dimethyl Ether, 2021. doi:10.48550/arXiv.2105.13175 (accessed 6 March 2025).
[57] S.-J. Kim, P.S. Lee, M.-J. Park, D.-W. Lee, Y.-I. Park, S.-E. Nam, K.-H. Lee, DME conversion using high flux tubular membrane reactors, Sep. Sci. Technol. 51 (2016) 2062–2069, https://doi.org/10.1080/01496395.2016.1198378.

[58] J.-X. Lin, W.-J. Wang, B.-Y. Yu, C.W. Ong, C.-L. Chen, Intensification of the CO2-capturing methanol steam reforming process: a comprehensive analysis of energy, economic and environmental impacts, Sep. Purif. Technol. 347 (2024) 127612, https://doi.org/10.1016/j.seppur.2024.127612.

[59] C.W. Ong, J.-X. Lin, M.-L. Tsai, K.S. Thoe, C.-L. Chen, Techno-economic and carbon emission analyses of a methanol-based international renewable energy supply chain, Int. J. Hydrog. Energy 49 (2024) 1572–1585, https://doi.org/10.1016/j.ijhydene.2023.10.191.

[60] P. Häussinger, R. Lohmüller, A.M. Watson, Hydrogen, 2. Production, in: Ullmann's Encyclopedia of Industrial Chemistry, Wiley, Chichester, 2010.

[61] M.A. Crews, B.G. Shumake, Hydrogen production, in: C.S. Hsu, P.R. Robinson (Eds.), Springer Handbook of Petroleum Technology, Enhanced Credo edition, Springer, Cham, Switzerland, Boston, Massachusetts, 2019, pp. 787–816. Credo Reference.

[62] S.A. Treese, Hydrogen production and management for petroleum processing, in: S.A. Treese, D.S. Jones, P.R. Pujado (Eds.), Handbook of Petroleum Processing, Springer International Publishing; Springer, Cham, 2019, pp. 1–67.

[63] J. Rostrup-Nielsen, L.J. Christiansen, Concepts in Syngas Manufacture, Imperial College Press, 2011.

[64] C. Murkin, J. Brightling, Eighty Years of Steam Reforming 60, Johnson Matthey Technology Review, 2016, pp. 263–269, https://doi.org/10.1595/205651316X692923.

[65] M. Bui, C.S. Adjiman, A. Bardow, E.J. Anthony, A. Boston, S. Brown, P.S. Fennell, S. Fuss, A. Galindo, L.A. Hackett, J.P. Hallett, H.J. Herzog, G. Jackson, J. Kemper, S. Krevor, G.C. Maitland, M. Matuszewski, I.S. Metcalfe, C. Petit, G. Puxty, J. Reimer, D.M. Reiner, E.S. Rubin, S.A. Scott, N. Shah, B. Smit, J.P.M. Trusler, P. Webley, J. Wilcox, N. Mac Dowell, Carbon capture and storage (CCS): the way forward, Energy Environ. Sci. 11 (2018) 1062–1176, https://doi.org/10.1039/C7EE02342A.

[66] G.T. Rochelle, Amine scrubbing for CO2 capture, Science 325 (2009) 1652–1654, https://doi.org/10.1126/science.1176731.

[67] M.A. Khan, C. Young, C. MacKinnon, D. Layzell, The Techno-Economics of Hydrogen Compression, Transition Accelerator Technical Briefs 1, 2021, pp. 1–36. https://transitionaccelerator.ca/wp-content/uploads/2023/04/TA-Technical-Brief-1.1_TEEA-Hydrogen-Compression_PUBLISHED.pdf. (Accessed 26 February 2025).

[68] A.M. El Hajj Chehade, E.A. Daher, J.C. Assaf, B. Riachi, W. Hamd, Simulation and optimization of hydrogen production by steam reforming of natural gas for refining and petrochemical demands in Lebanon, Int. J. Hydrog. Energy 45 (2020) 33235–33247, https://doi.org/10.1016/j.ijhydene.2020.09.077.

[69] P. Strucks, L. Failing, S. Kaluza, A short review on Ni-catalyzed methanation of CO 2 reaction mechanism, catalyst deactivation, dynamic operation, Chemie Ingenieur Technik 93 (2021) 1526–1536, https://doi.org/10.1002/cite.202100049.

[70] C.N. Hinshelwood, P.J. Askey, Homogeneous reactions involving complex molecules.—the kinetics of the decomposition of gaseous dimethyl ether, Proc. R. Soc. Lond. A 115 (1927) 215–226, https://doi.org/10.1098/rspa.1927.0087.

[71] D.J. McKenney, K.J. Laidler, KInetics and mechanisms of the pyrolysis of dimethyl ether: I. The uninhibited reaction, Can. J. Chem. 41 (1963) 1984–1992, https://doi.org/10.1139/v63-291.

[72] G. Garbarino, F. Pugliese, T. Cavattoni, G. Busca, P. Costamagna, A study on CO2 methanation and steam methane reforming over commercial Ni/calcium aluminate catalysts, Energies 13 (2020) 2792, https://doi.org/10.3390/en13112792.

[73] X. Hu, G. Lu, Inhibition of methane formation in steam reforming reactions through modification of Ni catalyst and the reactants, Green Chem. 11 (2009) 724, https://doi.org/10.1039/B814009J.

[74] L. Oar-Arteta, A.T. Aguayo, A. Remiro, A. Arandia, J. Bilbao, A.G. Gayubo, Kinetics of the steam reforming of dimethyl ether over CuFe2O4/γ-Al2O3, Chem. Eng. J. 306 (2016) 401–412, https://doi.org/10.1016/j.cej.2016.07.075.

[75] EIGA, Best Available Techniques for Hydrogen Production by Steam Methane Reforming: Doc 155/21. https://www.eiga.eu/uploads/documents/DOC155.pdf. (Accessed 4 June 2025).

[76] Johnson Matthey, Steam Reforming Catalysts: Natural Gas, Associated Gas and LPG. https://matthey.com/documents/161599/348563/JM+Steam+reforming+catalysts+Product+Brochure.pdf/99deb020-f1af-f436-c6b3-a3557ad2499e?t=1664979352415. (Accessed 4 June 2025).

[77] Linde, Hydrogen, in: https://assets.linde.com/-/media/global/engineering/engineering/home/products-and-services/process-plants/h2_1_1_e_12_150dpi_nb.pdf. (Accessed 26 February 2025).

[78] D. Maporti, S. Guffanti, F. Galli, P. Mocellin, G. Pauletto, Towards sustainable hydrogen production: integrating electrified and convective steam reformer with carbon capture and storage, Chem. Eng. J. 499 (2024) 156357, https://doi.org/10.1016/j.cej.2024.156357.

[79] DIN EN ISO 16903, Erdöl- und Erdgasindustrie — Eigenschaften von Flüssigerdgas mit Einfluss auf die Auslegung und die Materialauswahl, 2015.

[80] ISO 16861, Petroleum Products - Fuels - Specifications of Dimethyl Ether, 2015.

[81] L. Mosca, E. Palo, M. Colozzi, G. Iaquaniello, A. Salladini, S. Taraschi, Hydrogen in chemical and petrochemical industry, in: Current Trends and Future Developments on (Bio-) Membranes, Elsevier, 2020, pp. 387–410.

[82] EIGA, Combustion Safety for Steam Reformer Operation: Doc 172/24. https://www.eiga.eu/ct_documents/doc172-pdf/, 2024. (Accessed 6 March 2025).

[83] F. Rosner, Q. Chen, A. Rao, S. Samuelsen, Thermo-economic analyses of isothermal water gas shift reactor integrations into IGCC power plant, Appl. Energy 277 (2020) 115500, https://doi.org/10.1016/j.apenergy.2020.115500.

[84] W. Boll, G. Hochgesand, C. Higman, E. Supp, P. Kalteier, W.-D. Müller, M. Kriebel, H. Schlichting, H. Tanz, Gas Production, 3. Gas Treating, in: Ullmann's Encyclopedia of Industrial Chemistry, Wiley, 2003.

[85] O.C. Leite, Submerged Combustion Vaporisers for LNG Distribution Facilities: Submerged Combustion Vaporisers, Used to Vaporise LNG Stored Under Low Temperature, Are Ideal for Peak Shaving and Base Load Facilities. https://cdn.digitalrefining.com/data/articles/file/171194535.pdf. (Accessed 7 March 2025).

[86] A. Singh, K. Stéphenne, Shell Cansolv CO2 capture technology: achievement from first commercial plant, Energy Procedia 63 (2014) 1678–1685, https://doi.org/10.1016/j.egypro.2014.11.177.

[87] U.S. Department of Energy, Phase II / III Review: Large Pilot Testing of Linde-BASF Advanced Post-Combustion CO2 Capture Technology at a Coal-Fired Power Plant (FE-0031581). https://netl.doe.gov/sites/default/files/netl-file/21CMOG_PSC_Brownstein.pdf. (Accessed 6 March 2025).

[88] U.S. Department of Energy, Combined Carbon Capture Solution on Air Liquide South Texas Steam Methane Reformer: Agreement No. DE-FE0032181. https://netl.doe.gov/sites/default/files/netl-file/24CM/24CM_PSCC_6_Odom.pdf. (Accessed 28 February 2025).

[89] U.S. Department of Energy, Compendium of Carbon Capture Technology. https://netl.doe.gov/sites/default/files/2025-01/Carbon-Capture-Compendium-2024.pdf, 2024. (Accessed 28 February 2025).

[90] H. Barlow, S.S.M. Shahi, State of the Art: CCS Technologies. https://www.globalccsinstitute.com/wp-content/uploads/2024/08/CCS-Technologies-Compendium-2024-08-16-1.pdf, 2024. (Accessed 28 February 2025).

[91] M. Bertau, H. Offermanns, L. Plass, F. Schmidt, H.-J. Wernicke, Methanol: The Basic Chemical and Energy Feedstock of the Future, Springer Berlin Heidelberg, Berlin, Heidelberg, 2014.

[92] API, API Recommended Practice 538: Industrial Fired Boilers for General Refinery and Petrochemical Service.

[93] V. Ganapathy, Understanding boiler circulation, J. Chem. Eng. (2013) 52–58.

[94] IEAGHG, IEAGHG Technical Report 2017–02: Techno - Economic Evaluation of SMR Based Standalone (Merchant) Hydrogen Plant with CCS. https://ieaghg-publications.s3.eu-north-1.amazonaws.com/Technical+Reports/2017-02+Techno+-+Economic+Evaluation+of+SMR+Based+Standalone+(Merchant)+Hydrogen+Plant+with+CCS.pdf, 2017. (Accessed 6 March 2025).

[95] P. Liley, G. Thomson, D.G. Friend, T. Daubert, E. Buck, Physical and chemical data, in: Perry's Chemical Engineers' Handbook, seventh. ed, McGraw-Hill, New York, NY, 1999, pp. 25–398.

[96] P. Schühle, R. Stöber, M. Semmel, A. Schaadt, R. Szolak, S. Thill, M. Alders, C. Hebling, P. Wasserscheid, O. Salem, Electronic supplementary information: dimethyl ether/CO 2 – a hitherto underestimated H 2 storage cycle, Energy Environ. Sci. (2023), https://doi.org/10.1039/D3EE00228D.

[97] L.T. Biegler, I.E. Grossmann, A.W. Westerberg, Systematic Methods of Chemical Process Design, Prentice Hall PTR, New Jersey, 1999.

[98] J.R. Couper, W.R. Penney, J.R. Fair, Chemical Process Equipment: Selection and Design, second edition, Butterworth-Heinemann, Burlington, USA, 2010.

[99] J. Sundberg, S. Rehfeldt, A. Peschel, H. Klein, Process optimization of the methanol synthesis using different local optimization algorithms, Chem. Ing. Tech. 89 (2017) 675–685, https://doi.org/10.1002/cite.201600108.

[100] I.D.G. Chaves, J.R.G. López, J.L.G. Zapata, A.L. Robayo, G.R. Niño, Process optimization in chemical engineering, in: I.D. Gil Chaves, J.R.G. López, J. L. García Zapata, A. Leguizamón Robayo, G. Rodríguez Niño (Eds.), Process Analysis and Simulation in Chemical Engineering, Springer International Publishing, Cham, 2016, pp. 343–369.

[101] T.N. From, B. Partoon, M. Rautenbach, M. Østberg, A. Bentien, K. Aasberg-Petersen, P.M. Mortensen, Electrified steam methane reforming of biogas for sustainable syngas manufacturing and next-generation of plant design: a pilot plant study, Chem. Eng. J. 479 (2024) 147205, https://doi.org/10.1016/j.cej.2023.147205.

[102] A.-M. Ecker, H. Klein, A. Peschel, Systematic and efficient optimisation-based design of a process for CO2 removal from natural gas, Chem. Eng. J. 445 (2022) 136178, https://doi.org/10.1016/j.cej.2022.136178.